2008

Devising a more robust automated detection method using audio frequency spectra

Gregory Stargell
Iowa State University

Devising a more robust automated detection method using audio frequency spectra

by

Gregory Stargell

A thesis submitted to the graduate faculty

in partial fulfillment of the requirements for the degree of

MASTER OF SCIENCE

Major: Mechanical Engineering

Program of Study Committee:
J. Adin Mann III, Major Professor
Thomas J. Rudolphi
Michael B. Pate

Iowa State University
Ames, Iowa
2008

UMI Number: 1453059

ProQuest Information and Learning Company
300 North Zeeb Road
P.O. Box 1346
Ann Arbor, MI 48106-1346

Table of Contents

Chapter 1: Introduction

The National Aeronautical and Space Administration (NASA) space program has been significantly affected by the tragic accidents of the space shuttle. The cause of one of the calamitous accidents was the thermal insulation foam being dislodged during launch. Extensive resources, by some accounts over one billion dollars, has been spent to solve this problem. The information provided in this thesis will describe the efforts to improve on a potential technique to identify flaws in the application of the thermal insulation called Spray on Foam Insulation or SOFI for short.

1.1 SOFI Hazard Background

5, 4, 3, 2, 1….The countdown for the launch of Columbia on January 16, 2003 for a microgravity and Earth Science research mission at the Kennedy Space Flight Center in Florida. The STS-107 in which included Rick Husband (commander), Willie McCool (pilot), Michael P. Anderson, Laurel B. Clark, and David M. Brown, the first Israeli astronaut, Ilan Ramon, and the first female Indian astronaut, Kalpana Chawla. During their return on February 1, 2003, NASA lost radio transmission with the Columbia at 9:00 A.M Eastern Standard Time. There has been media showing that the Columbia burst into flames over Texas at a speed over 12,000 mph (5.0 km/s). After months of investigation on the space shuttle, it was concluded that a hole was punctured into the wing of space ship which was caused by a piece of the SOFI the size of a suitcase falling off the propellant tank of the space shuttle, Figure 1.1. The hole caused by the SOFI at lift off caused hot gases to enter

the wing which destroyed the support structure, and unfortunately lead to the demise of the space shuttle and the astronauts due to the intense heat of entering the Earth's atmosphere.

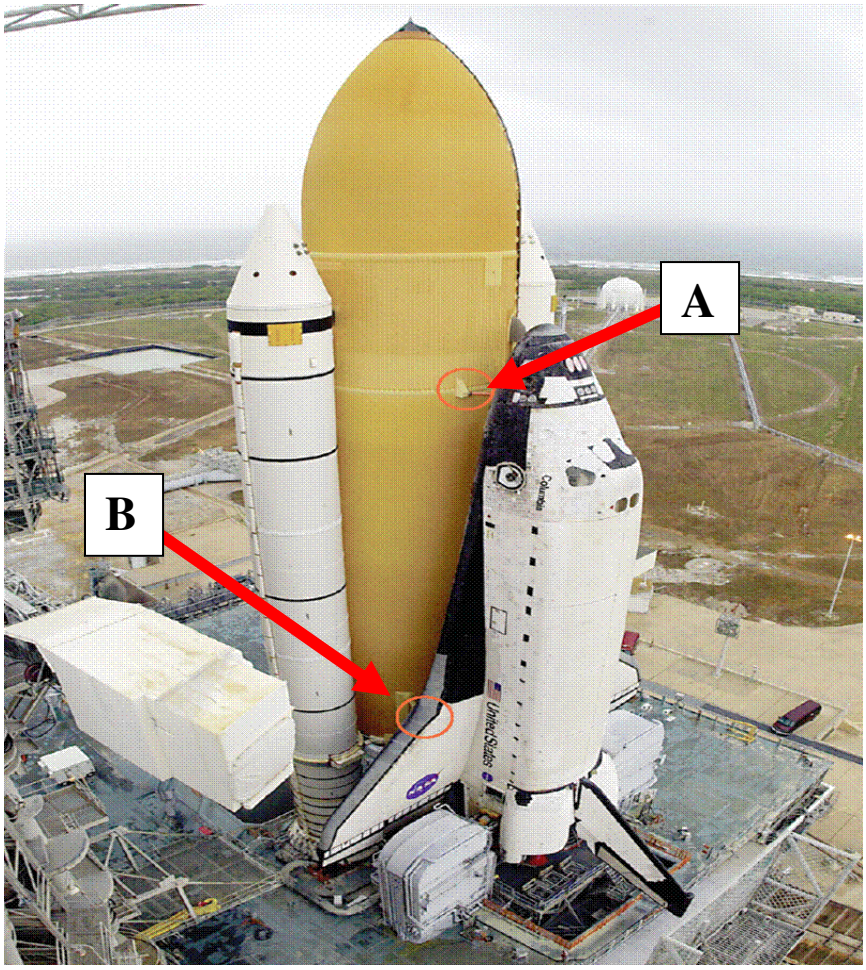

Figure 1.1: The Columbia Space Shuttle during liftoff. The circle represented by the letter A is the area where the foam fell and hit the shuttle wing at the location which is represented by the circle, B.

On July 26, 2005, another incident with the foam occurred, this time with the space shuttle, Discovery (STS- 114). After liftoff and after the Space Shuttle Solid Rocket Booster

separation, a piece of the SOFI compared to be half the size of the one that fell off the Columbia come off the Protuberance Air Load (PAL) which is apart of the external tank as well, Figure 1.2. The significance of this instance is that the piece that fell off the tank was in a similar region as the Columbia. However unlike the Columbia, the SOFI did not impact hit any part of the orbiter (Chien, 2006). This caused NASA to postpone the mission on July 27, 2005 to investigate what is causing the foam to detach.

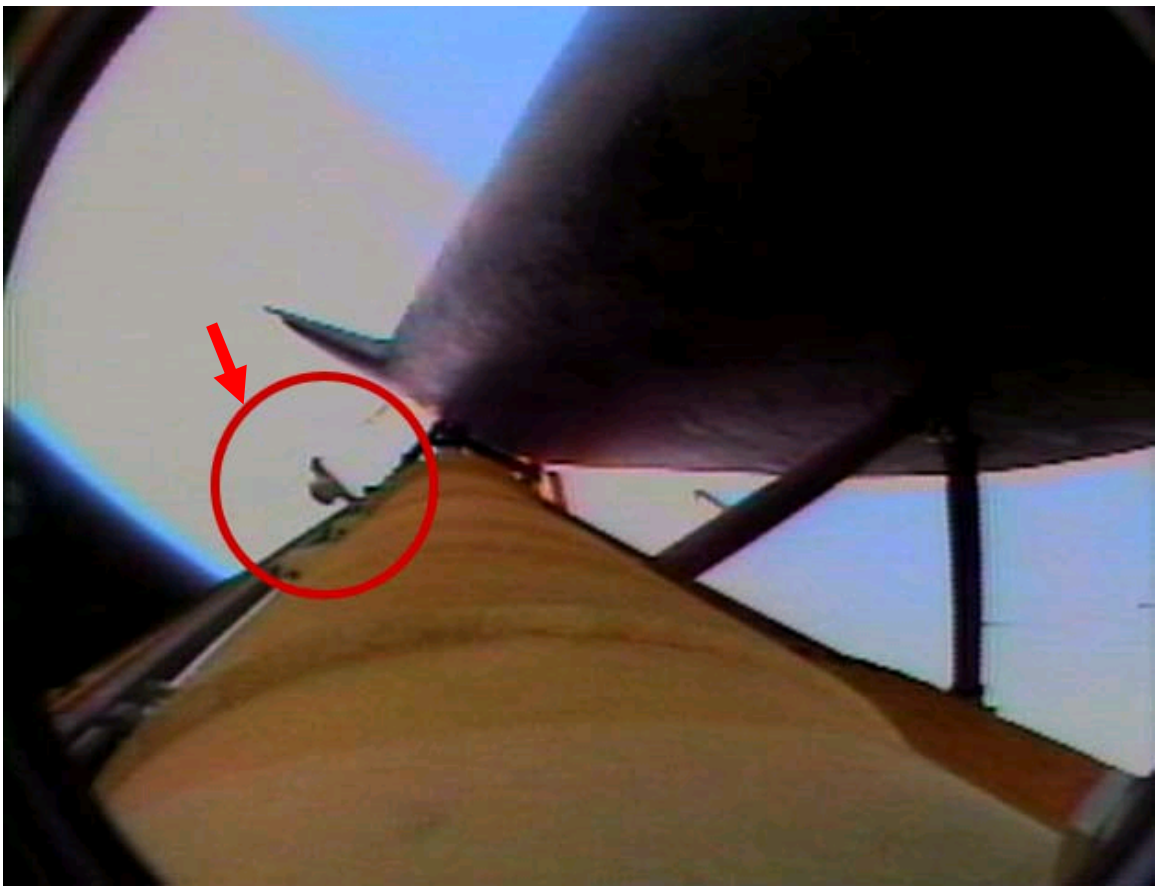

Figure 1.2: The space shuttle Discovery with a piece of the SOFI detaching from the PAL.

While SOFI falling during lift off has reportedly occurred throughout the shuttle program, it was not considered a severe problem after several launches resulted in no significant problems. However the Colombia tragedy launched a large effort to solve the problem and then when it reoccurred with Discovery, NASA continued to allocate significant resources to alleviate the problem.

NASA engineers had isolated the cause of the SOFI dislodging to flaws in the foam that occurred while the foam was applied to the liquid fuel tank. The flaws were either voids representing a gas pocket, or cohesion failures. NASA examined strategies to both eliminate and detect if there are flaws in the foam. The work in this thesis describes part of an effort to detect the flaws so that the flawed foam could be replaced.

1.2 SOFI Inspection Strategies

NASA's strategy to inspect the SOFI was to develop an inspection method so that the entire SOFI surface could be inspected. Several of the challenges included:

1) Inspecting around irregular geometries
2) Inspecting around bolt heads
3) Inspecting foam that varied in thickness from four to eight inches.
4) Inspect all SOFI surfaces (the entire liquid fuel tank)
5) Perform the inspection in an acceptable amount of time
6) Have a technique verified and qualified for deployment in the space shuttle construction program

These incidents caused NASA to explore different methods to evaluate the foam for defects. The methods that were explore were X-ray backscattering, Ultrasonics, Terahertz, Laser Shearography, and Audio Frequency Sound Absorption. The first three techniques were well developed and could detect voids of varying sizes, but each needed further development. Also each of the first three methods implemented the use of equipment that was costly and was the size of a copier machine. This would require NASA to develop a robotic scanning system to move the large equipment over the entire liquid fuel tank surface. Eventually NASA chose and deployed one of these techniques.

The methodology described in this paper is under the area of Audio Frequency Sound Absorption. Audio Frequency Sound Absorption was a new method for this application and thus had significant development hurdles. However it was pursued as a viable option because of its portable size and low cost in comparison to the other techniques.

1.3 Audio Frequency Sound Absorption Technique Background

The Audio Frequency Sound Absorption Technique relies on a measurement of the sound absorption properties of the SOFI. The sound absorption coefficient is the ratio of the absorbed sound energy to incident sound energy, and is commonly used in noise control application to predict noise reduction generated by the materials. It is common in noise control applications to use air gaps in materials to generate high absorption coefficients in targeted frequency bands. This inspired the work to use the Audio Frequency Sound Absorption measurement to detect air gaps in the SOFI material.

The sound absorption coefficient can be measured in two modes. One is in a free field and the other is enclosed in an impedance tube. The free field technique was explored by Matt McKee (McKee, 2004). His work provided proof of concept results and background noise, but also showed sensitivity to the flaws in the SOFI sample.

Todd Thompson followed up with the development of the impedance tube method (Thompson, 2005). This is a well documented technique to use with signal processing applications, however minor modifications were made to optimize the equipment for the SOFI application. The device developed by Thompson, shown in Figure 1.3, consists of a hollow acrylic tube, a high frequency loudspeaker, two microphones, and a base to seal the tube to the SOFI sample. Thompson determined effective parameters for the tube length, diameter, and seal.

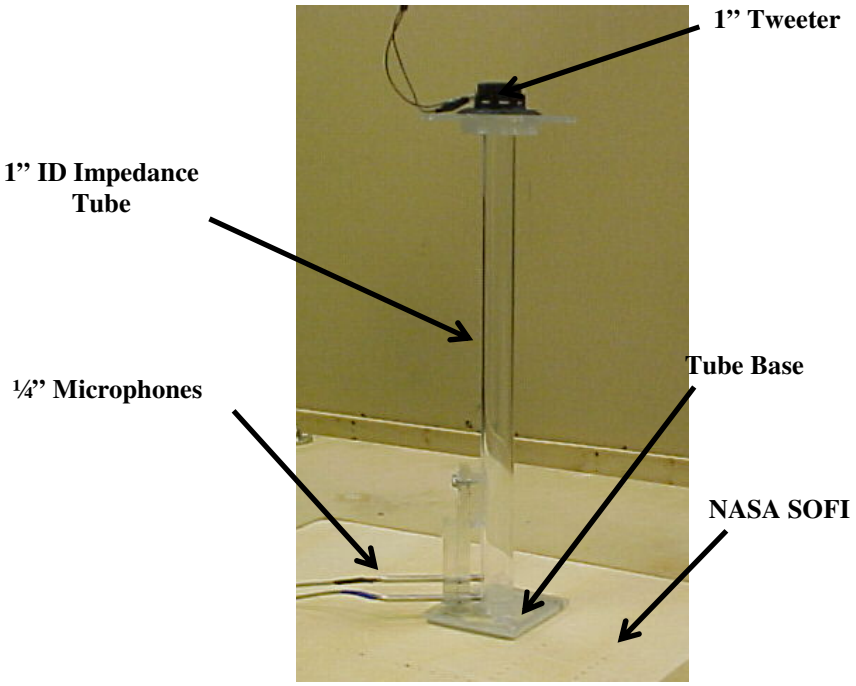

Figure 1.3: The Impedance tube developed by Todd Thompson (Thompson, 2005).

Figure 1.4, shows a comparison of the absorption coefficient using the free field technique implemented by McKee and the impedance tube (labeled in tube) technique implemented by Thompson. The smooth curve with the impedance tube technique shows how it is less affected by background noise. Other work by Thompson also showed that with the impedance tube technique significant amount of background noise did not change the measured absorption coefficient, making it useable in environments with high amounts of noise such as the manufacturing facility where the SOFI is applied to the liquid fuel tank.

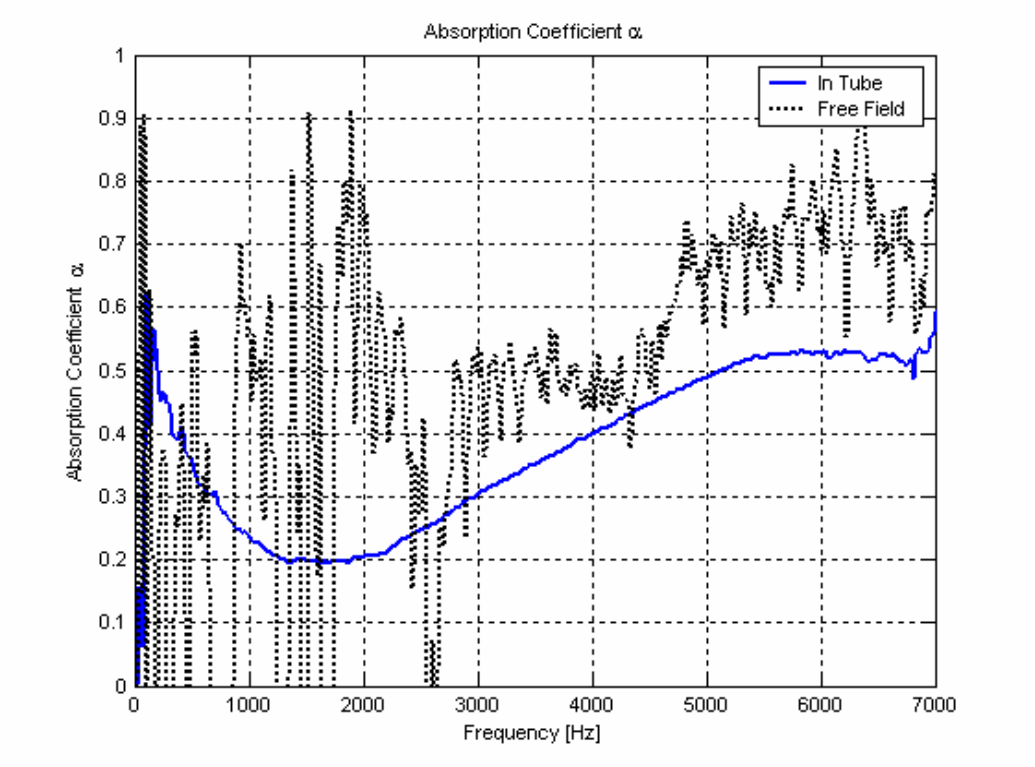

Figure 1.4: Example results for the free field and impedance tube measurements, showing the free field testing is very sensitive to its surroundings and background noise.

The impedance tube technique requires that the two microphone signals are measured and processed. A two channel data acquisition system was used. The equations and signal processing techniques are well documented by Thompson (Thompson, 2005). Since the data he acquired will be used in this thesis, the reader is referred to Thompson's thesis for the detailed explanation of the process.

The typical sound absorption spectra that were measured by Thompson are shown in Figure 1.5. Data over known defects, a 2 inch cut and 1 inch cut, are compared to data over a known bonded area. Over each of the defects, there are peaks in the absorption coefficient that clearly differentiate them from the bonded data. Thompson's detection technique therefore focused on developing a computer algorithm to quantify these peaks in the sound absorption spectra.

Thompson's indicator had mixed results. On a two inch thick sample, an indicator was developed that was used to identify two locations on the SOFI sample where the foam was disbonded from the metal substrate. This simulated a cohesive flaw.

Figure 1.6 shows the flaw indicator with its magnitude represented with a color plot, with the red color representing the flaw. The results show strong values at the locations of the two cohesive flaws that are located with the black rectangles on the upper and right side of the plot.

Based on the results documented in Thompson's thesis, the ISU research team was invited by NASA to participate in a study in which the capability and potential for inspection techniques considered viable at that time were compared. The process involved each research team was given a SOFI sample with embedded flaws. The sample that each team received had identical flaws.

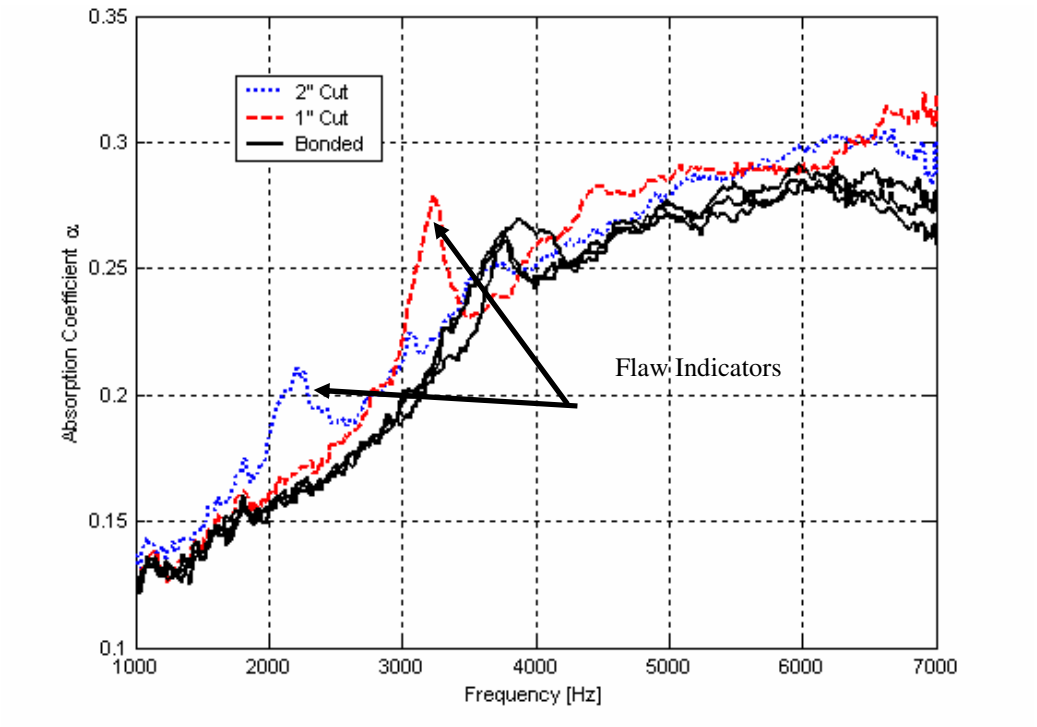

Figure 1.5: Example of measured absorption coefficient obtained by Thompson (Thompson, 2005).

Figure 1.7 shows a diagram provided by NASA giving the location and size of the flaw Note that all flaws are air pockets. In addition to the flaws, the metal structure had a shape that simulated parts on the liquid fuel tank, in this case a stiffening rib. The stiffening rib represents one of the key challenges with that all the inspection techniques were struggling.

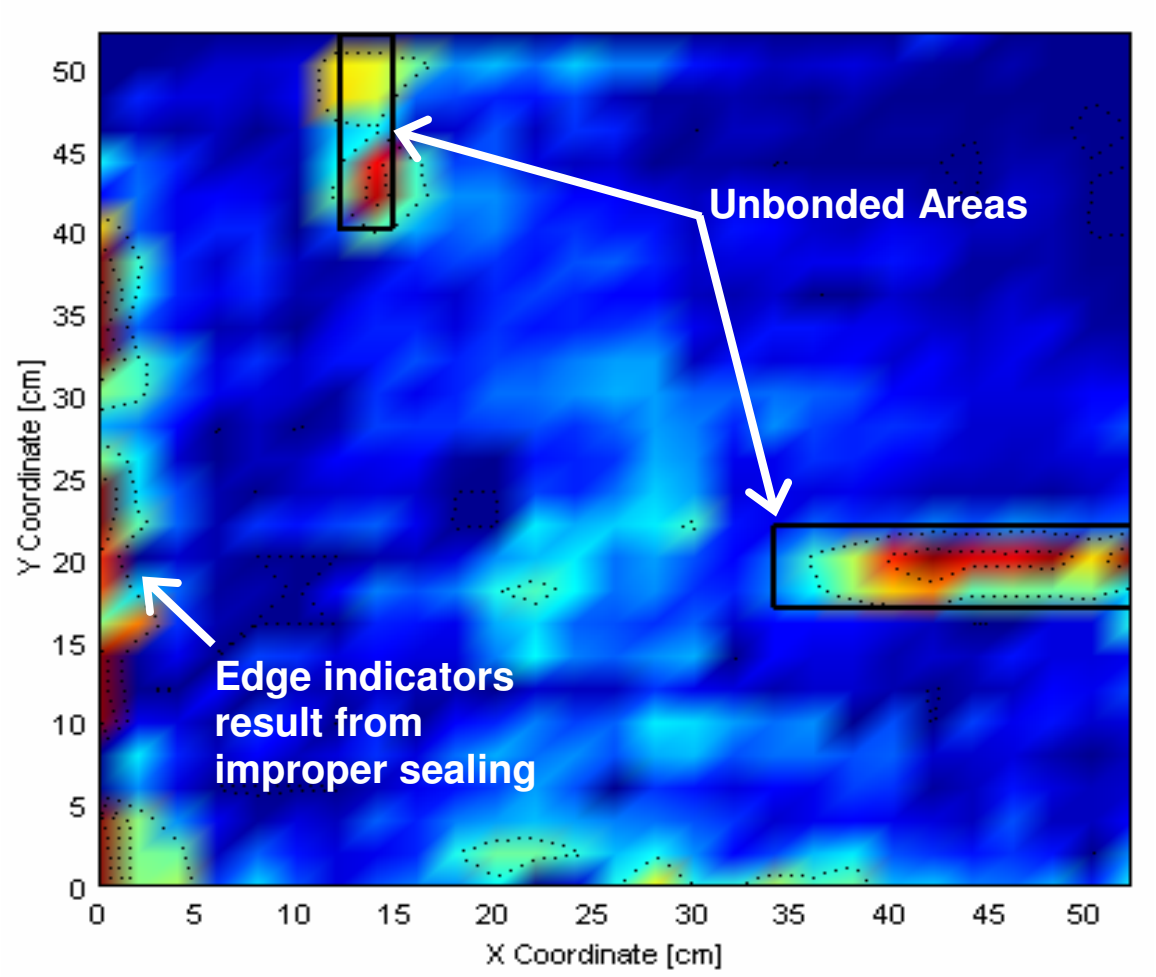

Figure 1.6: The regions where defects are located were depicted by the rectangles. Also there are some along the side due to the sealing error.

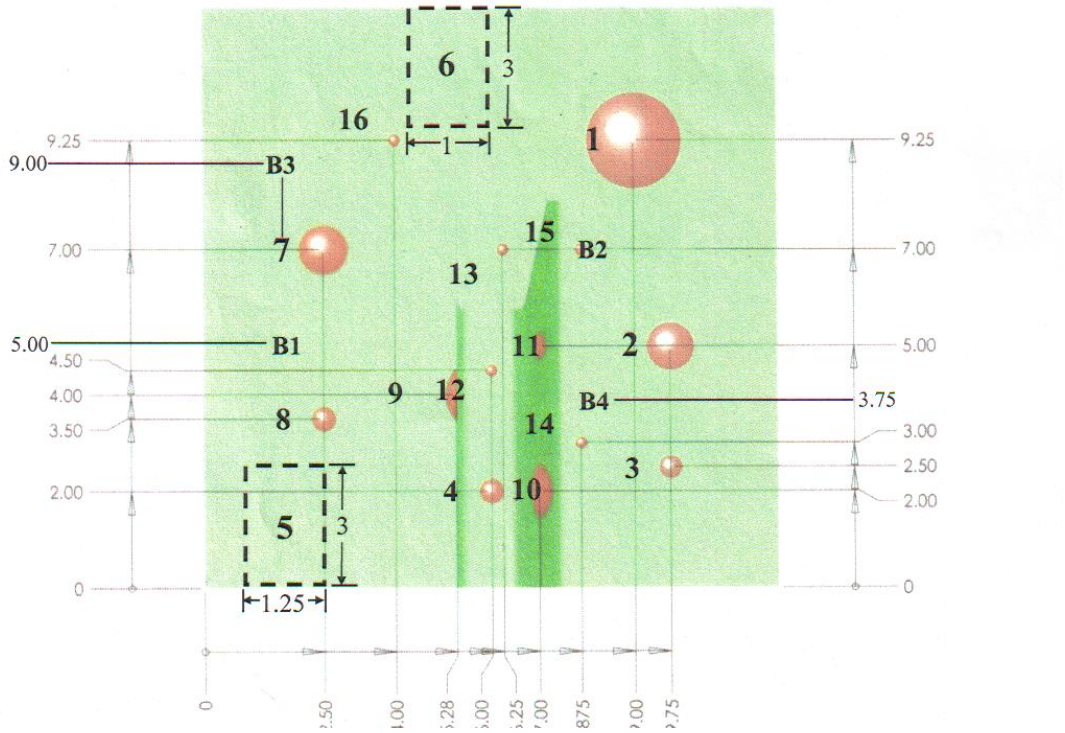

Figure 1.7: Diagram of each defects orientation, size, and 2-D location within the SOFI Sample.

In addition to the flaws created by NASA, Thompson created flaws that simulated cohesion failure. Figure 1.8 shows the added flaw and the measured absorption coefficient. It is worth knowing that the flaw is located two inches below the foam surface. Also between the range of 2500 Hz and 3000 Hz, there is a peak that stands out amongst the measured absorption coefficients. This peaks was not found in the regions where there were no defects or known defect.

The peaks seen in the data with the six inch thick sample did not produce peaks in the measured absorption data that were as strong as the two inch sample. One consequence was that the original flaw indicator developed by Thompson was not able to resolve all the

peaks that could be seen by visual inspection. Thompson developed a revised procedure to better quantify the changes in the impedance data over flaws in the six inch sample. This procedure will be described in more detail in Chapter 2.

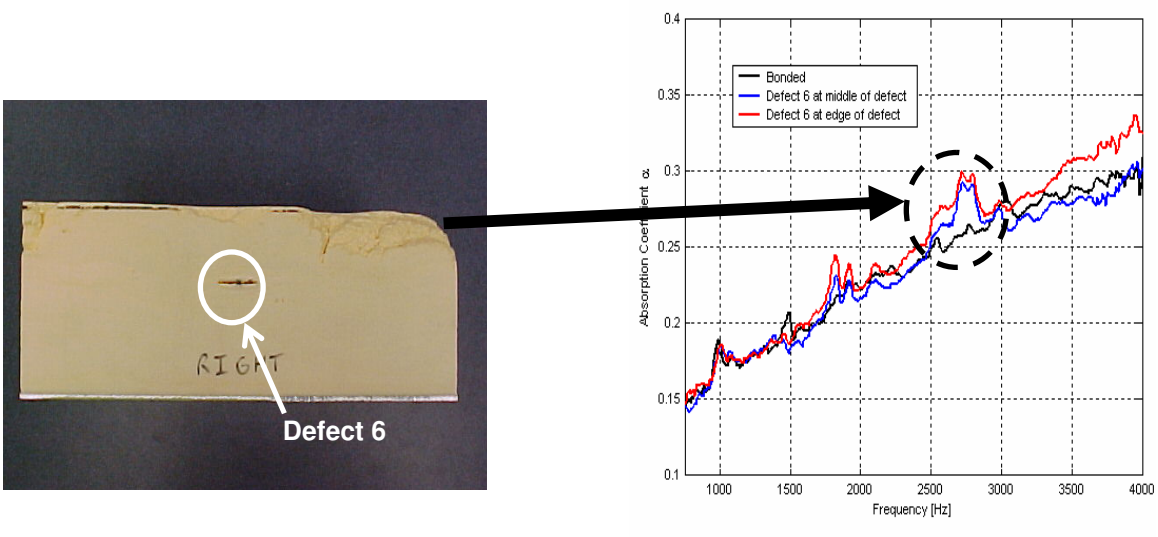

Figure 1.8: An example of a particular defect, and the data acquired from it.

Results from Thompson's revised indicator are shown in Figure 1.9. For these selected flaws the new indicator was effective. However as shown in Figure 1.10, the new indicator was not effective with all the flaws. Therefore, a more robust flaw indicator was needed to be developed.

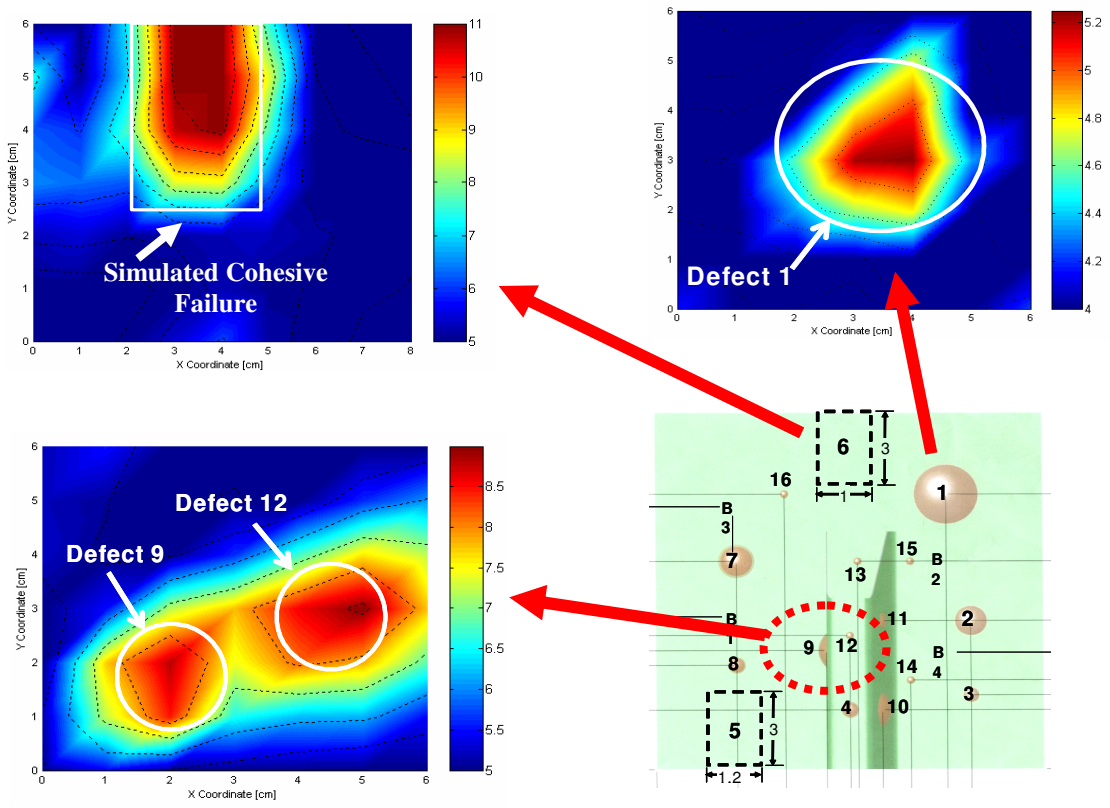

Figure 1.9: Flaw indicator results from Thompson for selected examples.. The bottom right is the defect mapping in the flaw. s

1.4 Research Goal and Thesis Outline

The research goal was to develop a new method to process the measured sound absorption to develop a more robust flaw indicator. The ultimate goal is to have the new method capable of detecting all the defects from the NASA sample as shown in Figure 1.7.

The thesis continues into Chapter 2 to provide a more detailed description of the processing that Thompson had developed. Analyzing the successes and failures of this

processing method and provides motivation for a revised method. Chapter continues by showing the new processing for a flaw indicator and shows results with a manual processing of data. Chapter 3 shows the development of an automated method for the new flaw indicator. The results of the new flaw indicator discussed in Chapter 4. Conclusions and recommendations for future work presented in Chapter 5.

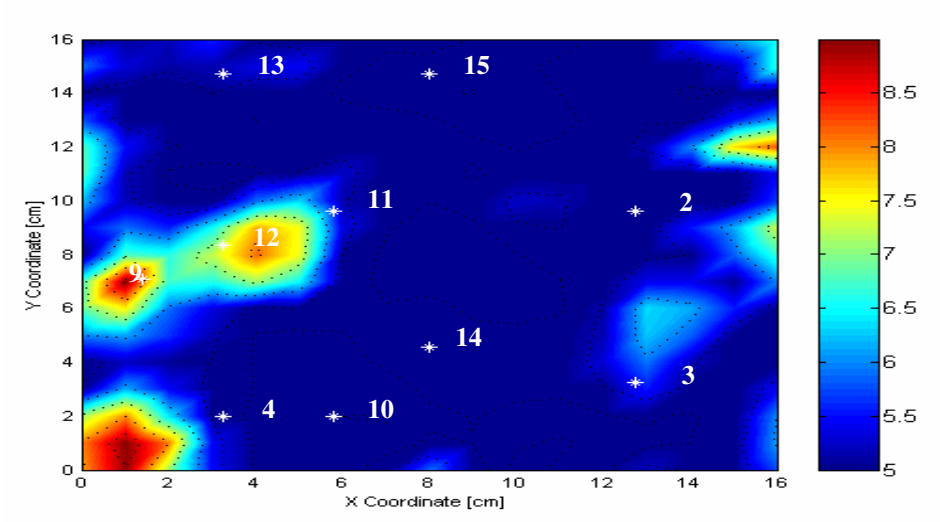

Figure 1.10: Defect 9 and 12 could be detected however the other defects would not be detected by Thompson's Method.

Chapter 2: Background and New Technique

As shown in Chapter 1, the sound absorption measurement is sensitive to flaws in the SOFI, however the current automated methods to extract that information has not been effective in all cases, where visual inspection could identify characteristics in the absorption spectra, such as peaks that are indicative of defects. Since the flaw detection method will be applied to situations where the sound absorption spectra will be evaluated at thousands of inspection points, it would not be possible to visually inspect that many points on spectra. Therefore an automated technique to identify flaws from the measured sound absorption spectra must be robust.

This chapter will describe the method developed by Thompson, focusing on where it failed in order to identify characteristics in the spectra that needed to be handled with a new inspection technique. From this, a new technique to present the sound absorption coefficient is presented.

2.1 Previous Methodology:

Thompson investigated two methods to detect the changes in the sound absorption spectra. The first was to directly compare the spectra at a location being evaluated to spectra from areas that are known to contain no flaws. The first technique relied upon the use of a reference spectrum with no flaw. Figure 2.1 shows measured absorption spectra of two points above known defects and four points above areas with no flaws. These results show a

consistent shape to the curves with deviations at peaks that can be clearly defined as a deviation from the data with no flaw.

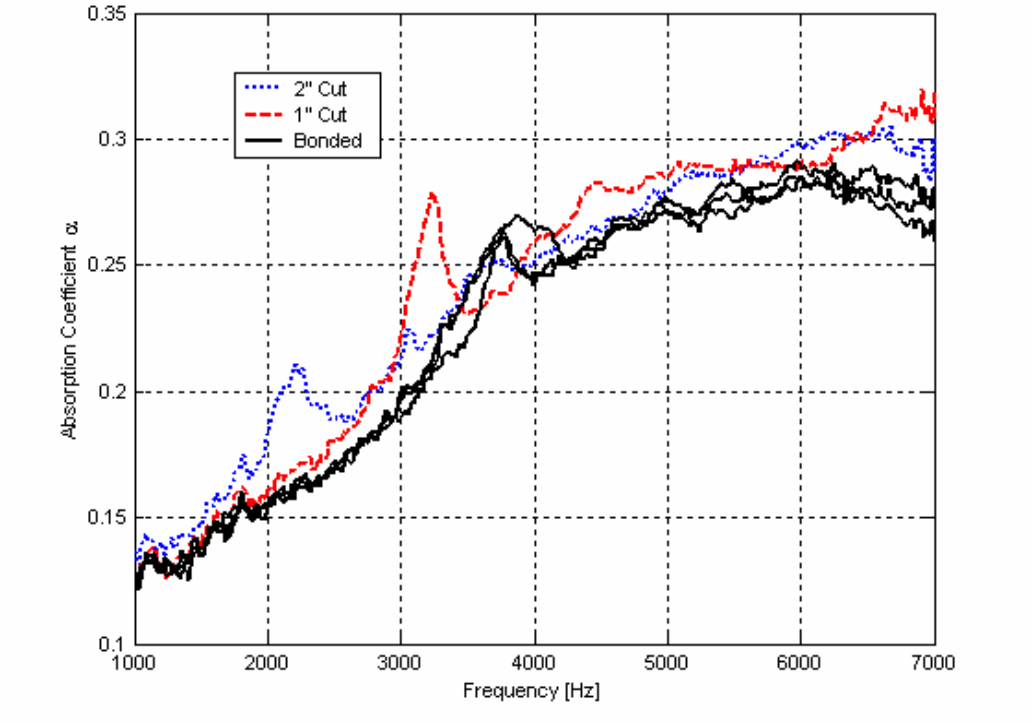

Figure 2.1: Measured absorption coefficient comparison of the thickness and the bonded region.

This technique was successful on the first SOFI sample that was only 2 inches thick with flaws that represent cohesive failures. However this approached failed with the thicker SOFI sample that contained flaws represented by voids or air pockets. Figure 2.2 shows part of the reason, the change between the base line shape of the data over an area with and without a flaw, has a baseline change that is equal to or more than the peak in the data over a flaw.

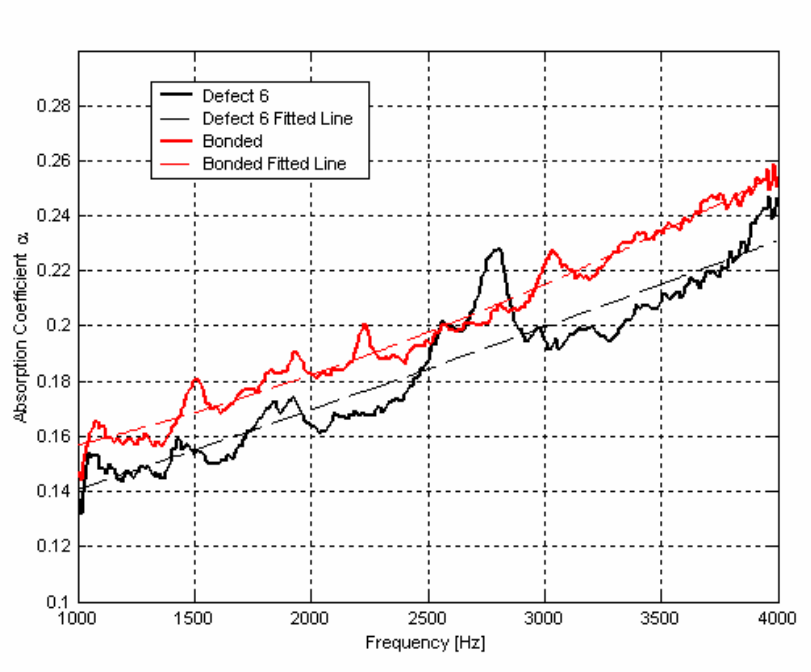

Figure 2.2: Deviation of the measured absorption coefficient of defect 6 and bonded region and the polynomial fit of each one in the dashed lines.

The second technique investigated by Thompson was based on the observation of data such as Figure 2.2 that the sound absorption spectra at points over a flaw and points over a bonded region (no flaw) had a base characteristic shape with peaks in the spectra over the flaw. While the amplitudes of each curve were different, the shape of the curve was consistent. Also it was the amplitude changes that made the first approach fail with the thicker SOFI sample. Therefore, Thompson developed a second technique that operated on individual spectra, without using a reference curve

The second method by Thompson began with fitting the measured sound absorption spectra by a second order polynomial. The second order fit was selected based on the evaluation of several spectra. An example of the measured data and the curve fit is shown in

Figure 2.3. Relative to the curve fit, the peak around 2700 Hz is a significant deviation from the curve fit.

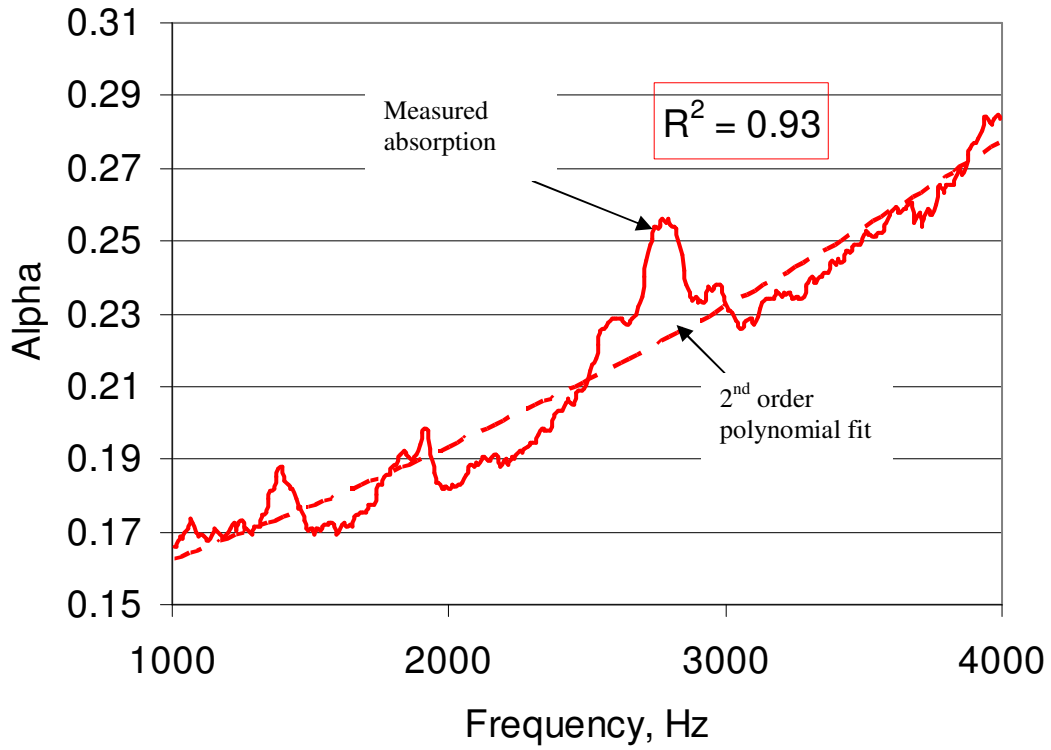

Figure 2.3: Measured absorption coefficient of Defect 6 with its second polynomial fit

Therefore in the next step of the data processing, the measured absorption coefficient was then subtracted by the polynomial fit and the difference then integrated over a specified frequency range or over the whole spectrum.

The result of the subtraction for the data in Figure 2.3 is shown in Figure 2.4. The peak around 2700 Hz is clearly the highest data points in Figure 2.4. This example is provided to show how the subtraction of the baseline curve fit enhances the identification of the peak associated with a flaw in the foam.

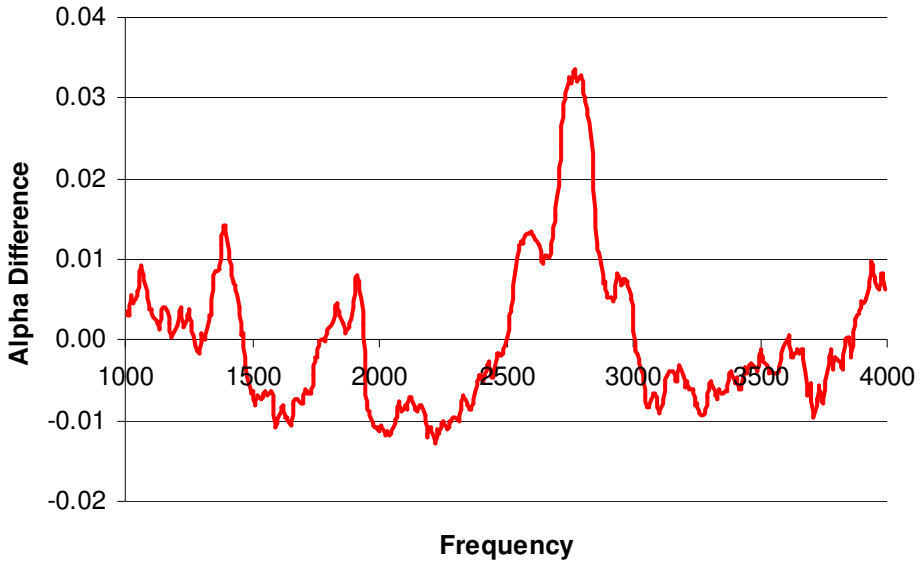

Figure 2.4: Deviation of the measured absorption coefficient and the polynomial fit.

However in reviewing Figure 2.3, one can see that that polynomial fit of the graph is influenced by the large peak in the data, in particular the peak around 2700 Hz. There are also peaks around 1400 Hz and 1800 Hz. These peaks also affect how well the curve fit will match the data, as indicated by the R-squared value. Figure 2.5, contains the measured absorption coefficient for another point along with the polynomial curve fit. One would notice that the R-squared value is 0.99, closer to a value of one which means that the behavior of the graph is fitted well by the polynomial

Visually, one can see in Figure 2.3 that there are much smaller peaks and therefore much less potential to influence the curve fit compared to Figure 2.1

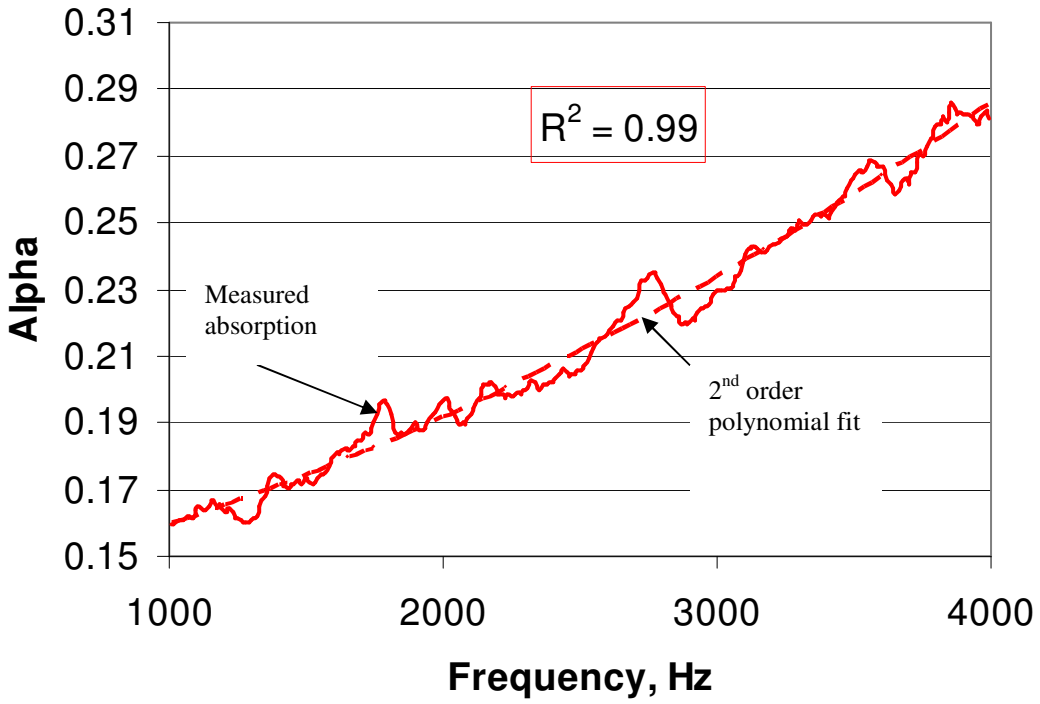

Figure 2.5: Measured absorption coefficient of one of the bonded regions with its second order polynomial fit.

Another issue with Thompson's second technique was that the frequency band over which the spectra were integrated was fixed. In the case of the data in Figure 2.3, a frequency range of 2500 Hz to 3000 Hz would be effective. However as shown in Figure 2.6, this frequency range would miss the peak around 3500 Hz.

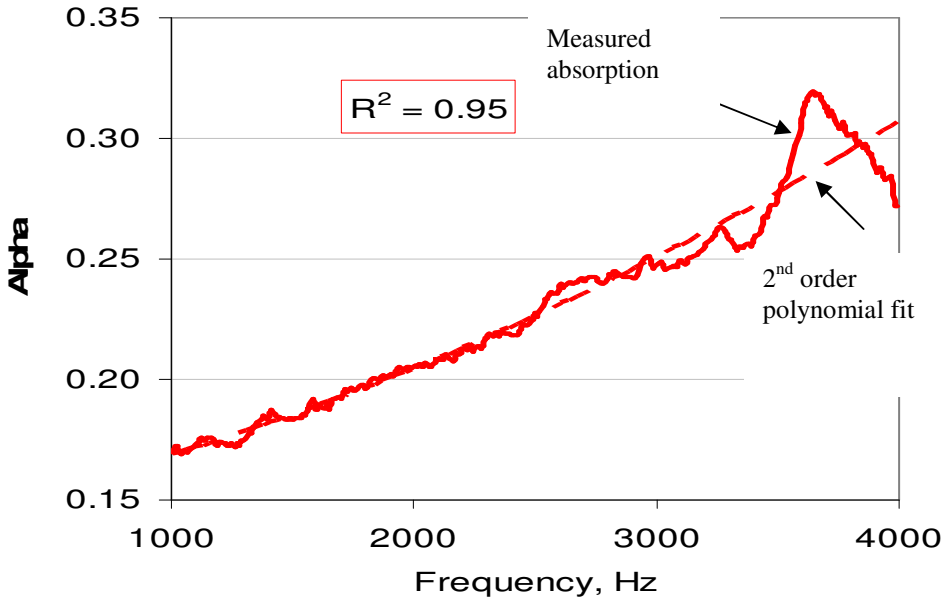

Figure 2.6: Measured absorption coefficient of Defect 9 with its second polynomial fit.

The review of the second technique by Thompson shows the basis of the technique was valid, but that typical data had features that were not fully captured.

Analysis showed that two issues needed to be addressed

- Reduce the influence of the peaks on the curve fit, so that the curve fit is to the underlying polynomial behavior of the material without a flaw.
- Integrate spectra over a frequency band that matches peaks in the spectra.

2.3 Proposed Methodology:

The proposed new methodology focused on the impact of the peaks on Thompson's second method. At the core of the proposed method is identifying the peaks so that:

- The peaks are not included in the spectra used in the curve fit.
- The spectra are integrated over the peaks

To begin, the influence of removing the peaks to enhance the curve fit will be discussed.

Consider as an example Figure 2.7, which contains a synthetic spectra with a large peak and the second order polynomial curve fit to the entire spectra. Clearly, the peak influences the curve fit from being a good representation of the base line curve. However if the peak is taken out and the second order polynomial fit is applied, Figure 2.8, that the polynomial fit now represent the curve which is known as the baseline.

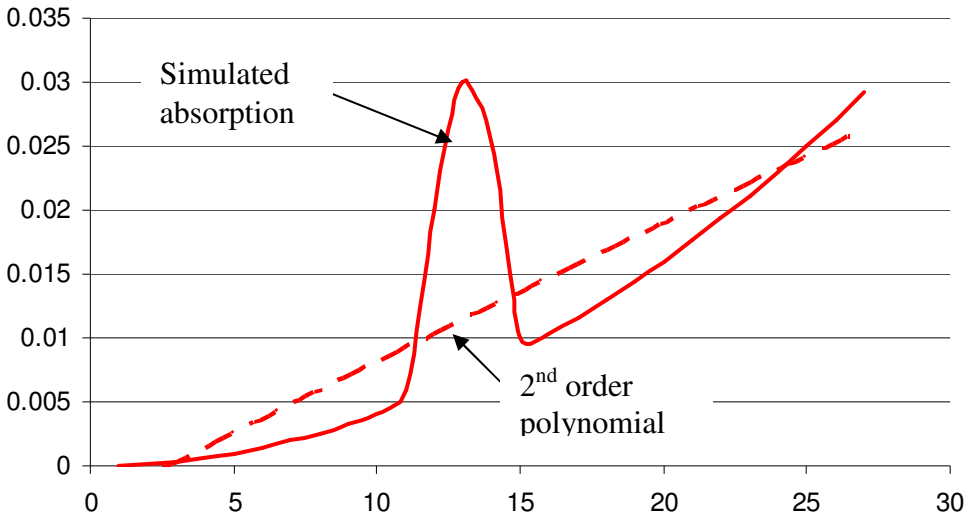

Figure 2.7: The polynomial fit the dashed lined represents the second order polynomial curve fit is heavily influenced by the peak in the data.

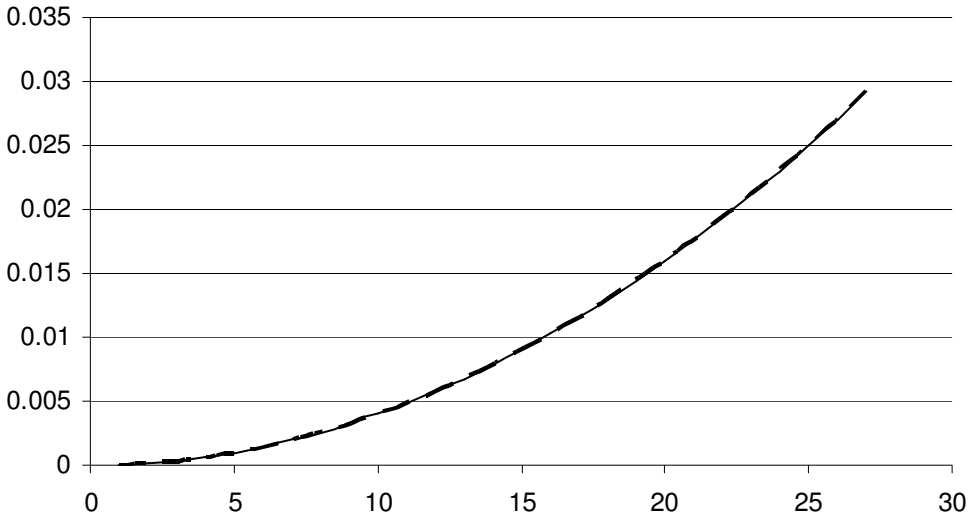

Figure 2.8: In comparison to Figure 2.7, it is obvious to see that when the peak is removed. The polynomial fit better represent the behavior of the curve.

Figure 2.9, shows the data given in Figure 2.3, but with an addition of the same curve that was generated by removing the peaks from the data. This was done manually in Excel. Figure 2.8 shows the original measured data again, along with the original second order polynomial curve fit. The third line is the second order polynomial curve fit to the original data with the peaks removed. The second curve fit shows a more improved representation of the baseline curve in the measured sound absorption coefficient.

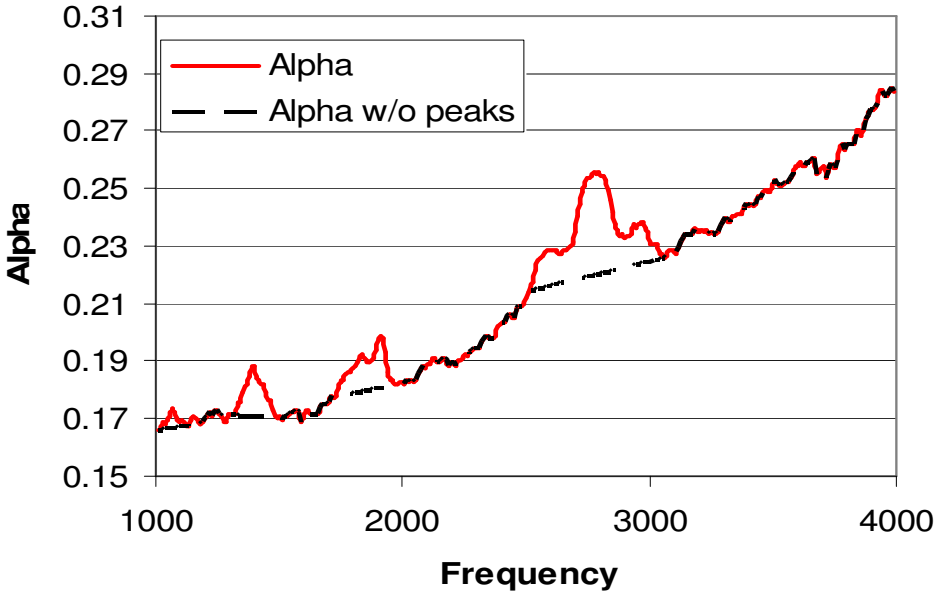

Figure 2.9: Comparison of the previous method and the current method on Defect 6.

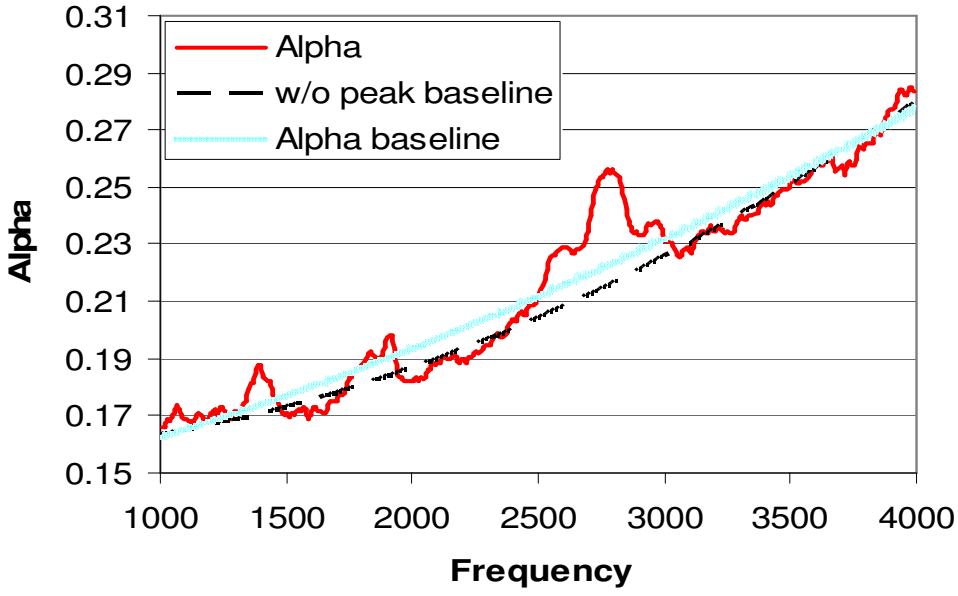

Figure 2.10: Comparison of the polynomial fit of the previous method (dashed line at the top) to the current method (The lower dashed line) on Defect 6.

Figure 2.9 and Figure 2.10, shows another example of the curve fit with the peak removed for the case of a single peak at the frequency around 3700 Hz. Again after removing the peak, the second order curve fit, Fig 2.10, is a better match to the baseline absorption curve.

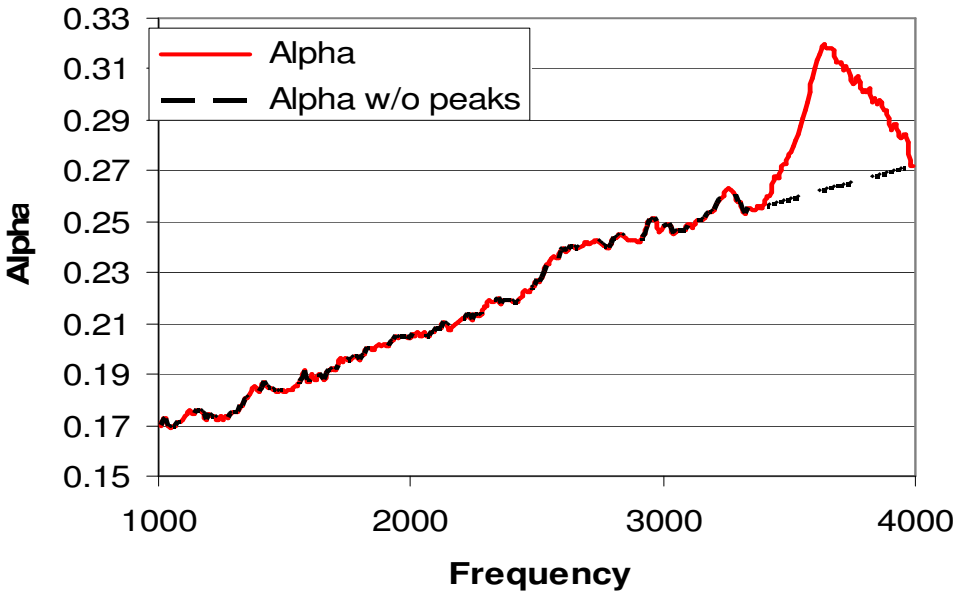

Figure 2.11: Comparison of the polynomial fit of the previous method (red) to the current method (black) on Defect 9.

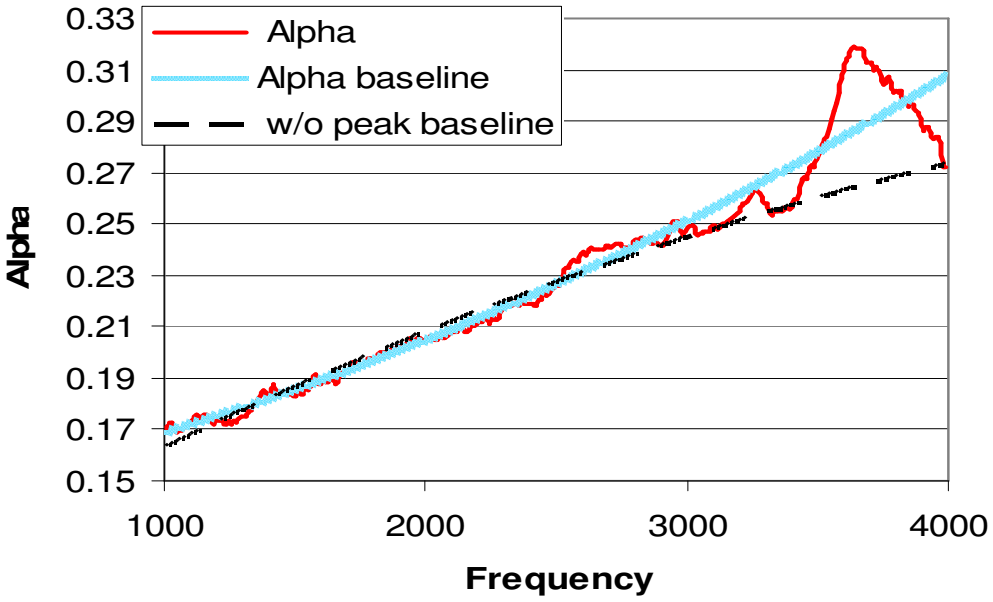

Figure 2.12: Comparison of the previous method and the current method on Defect 9.

Figures 2.13 and 2.14 show the difference between the measured data and each of the polynomial fits, one fit being Thompson's method to that included the peak and the other being the fit with the peak removed. In both cases the value of the peak is higher and the rest of the curve is closer to zero. Therefore these two cases show that by curve fitting after the peak removal, the peaks are better resolved.

The comparison of Figure 2.13 and 2.14 also emphasize the second improvement that is being proposed. Figure 2.14 has a frequency band labeled "Previous Range" that was a fixed frequency band over which the curves was integrated. While this frequency band will clearly work for the data point shown in Figure 2.13 it will not work for the data point in Figure 2.14. However since the process of removing the peak identifies the frequency range

of the peak this information can be used to establish the frequency band over which to integrate the data.

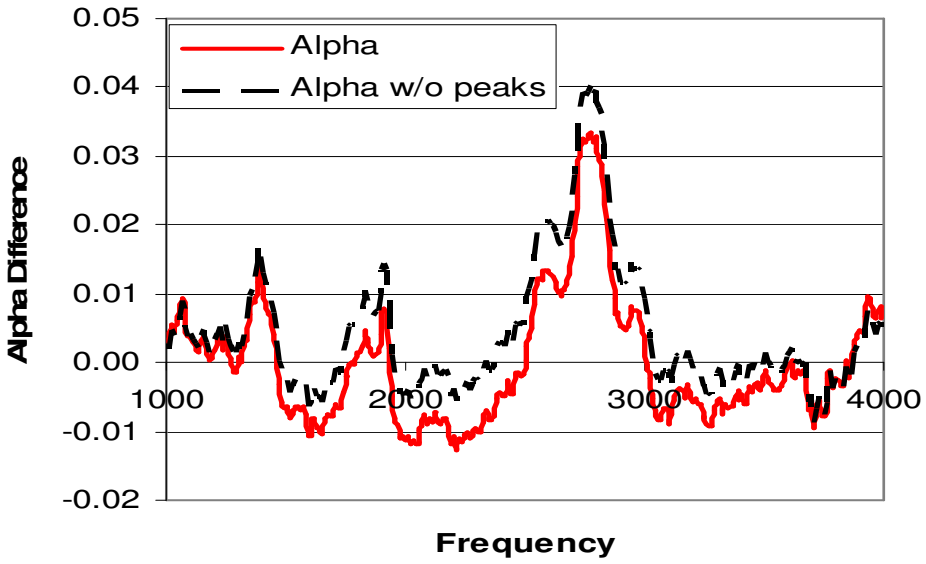

Figure 2.13: Comparison of the difference between the polynomial fits and the alpha values of defect 6. The proposed method is the top curve (Dark dash color) and the previous method is the lower curve (Light color).

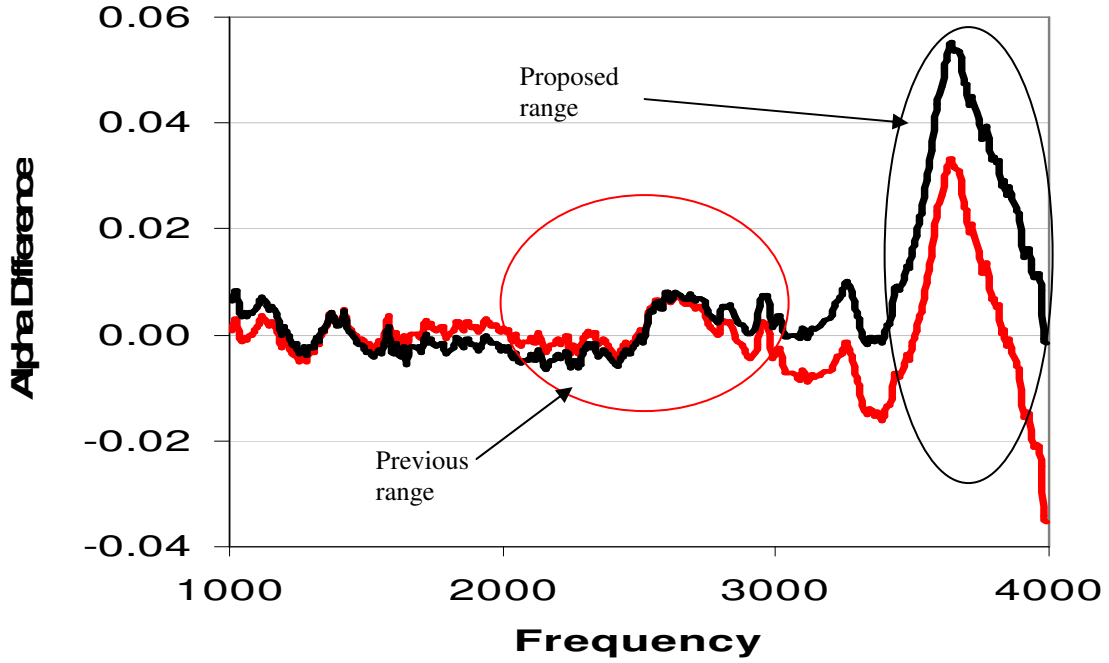

Figure 2.14: Comparison of the difference between the polynomial fits and the alpha values of defect 9. The proposed method is the top curve (Dark color) and the previous method is the lower curve (Light color).

The results of manual processing of data over 16 known defects and over 4 areas that were assumed to be bonded are presented in Figure 2.15 and 2.16. Figure 2.16 is the same data as presented in Figure 2.15 but with a smaller limit on the vertical axis to better show the results. In both figures the "Original" data refers to the processing as developed by Thompson, and "Modified" is the new proposed processing presented in this thesis.

The presentation of the data in Figure 2.14 is the most instructive. In all cases except defect 8, 14, 15, and 16, the new processing increased the value of the flaw indicator.

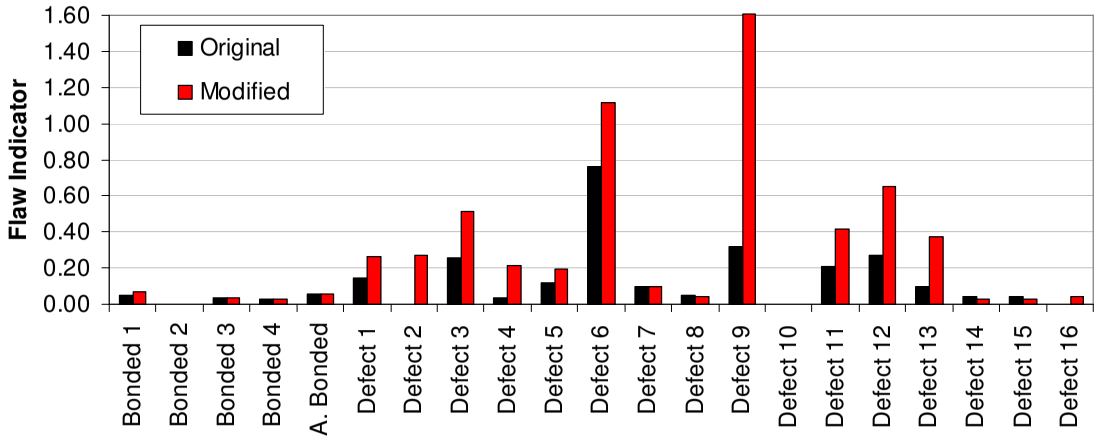

Figure 2.15: Comparison of Thompson's method (Original) to the proposed method (Modified)

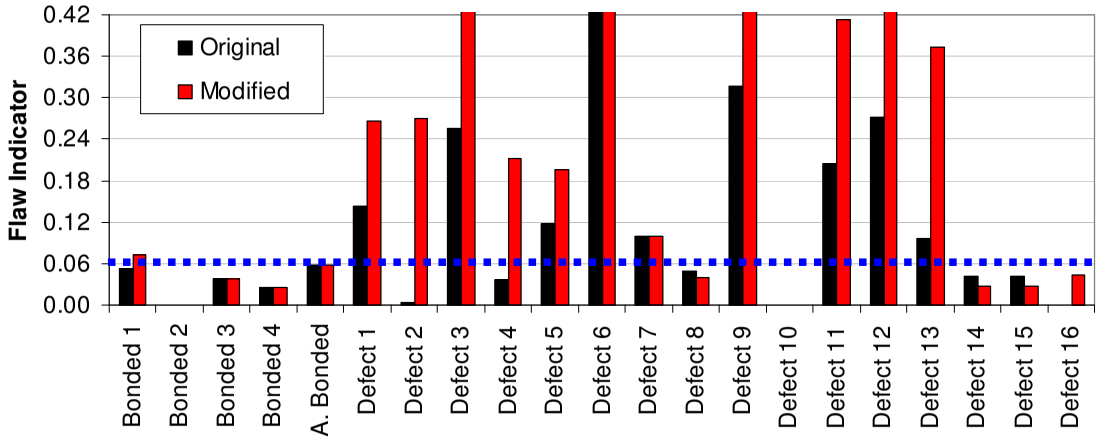

Figure 2.16: Repeat of Figure 2.15 with a smaller range on the flaw indicator to better show the differences.

Figure 2.16 has a horizontal dashed line that is set at the peak of the bonded data. This is set on the threshold that establishes a value for the flaw indicator that is above an examined value that can be obtained over a bonded region.

In the cases of defects 2 and 4, the Modified method made it possible for the defect to be detected which would not be detected using the "Original" method. In Defects 1, 3, 5, 6, 9, 11, 12, and 13, the value of the flaw indicator increased, making the identification of those defects more defined. In the case of defects 8, 10, 14, 15, and 16, as the new method did not improve the flaw indication, the flaws cannot be distinguished from the assumed bonded areas.

This new process was implemented manually searching through spectra. Once successful, the method must be implemented into an automated process However if as shown in Figure 2.11; the peak that was removed is in a different frequency range than that in Figure 2.9. Therefore evaluating the data over a particular frequency limit may not cause the spectra to be evaluated over a frequency range where the defect is actually located. This will be something to look into when make an automated process. Also notice how the when the peaks were removed the R-Squared value was 0.99, the same as for the bonded region.

Therefore the proposed method, which will be used in an automated process explained in the next chapter, will be to:

- Identify the frequency range of all peaks
- Remove the data from these frequency ranges.
- Curve fit the remaining spectra with a second order polynomial curve fit
- Subtract the curve fit from the original data
- Integrate the resulting spectra over the frequency bands of the peaks

Chapter 3: Automated Process

Evaluating the data using a manual process to remove peaks had improved flaw detection. However a manual process would not be suitable for full scans, because scans will have thousands of points. The task could get very tedious and time consuming. Therefore the peak removal and flaw detection calculations needed to be developed as an automated process. In order to develop strategies to approach this task, synthetic data was used first to simulate key features in the real data.

After developing data processing approaches using the synthetic data, the algorithms were applied to real data. The data processing approaches were then modified based on how the algorithms were affected by features in real data. The processing of real and synthetic data is presented in order to cut down on the amount of variables in the process, different cases of simplified data were made in order to see if the desired results can be obtained. The cases are: single peak, double peak, and special peak.

3.1 Synthetic Data:

The synthetic data was designed to focus on key features. The base was a second order polynomial. In the case of the data shown in Figure 3.1, the first synthetic data set added a single peak to the polynomial. In the second case, Figure 3.2, a second peak was added. In the third case, Figure 3.3, a peak was designed to have two maxima simulating a common feature in many of the spectra. Note that in Figures 3.1 to 3.3, the center frequency, band width, and magnitude of each peak was adjusted to represent this typical measured spectrum.

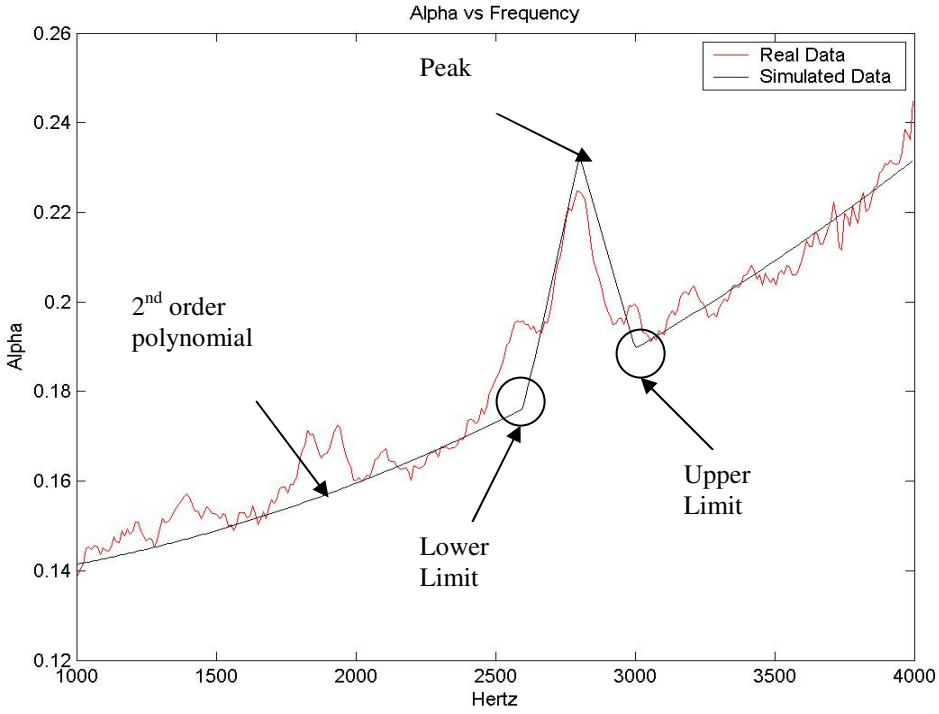

Figure 3.1: Example of synthetic data with a single peak with the real data.

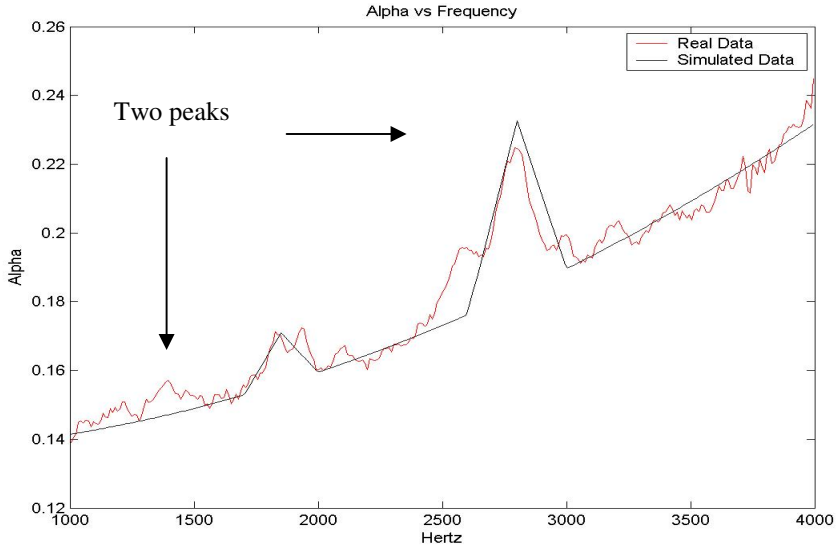

Figure 3.2: Example of synthetic data with two peaks with the real data.

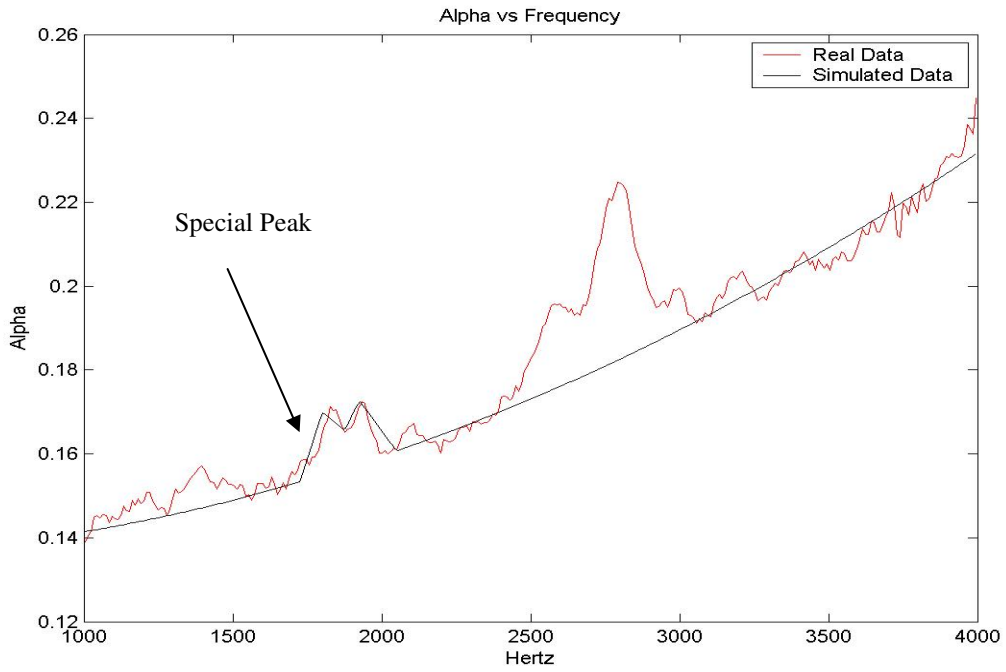

Figure 3.3: A comparison of the synthetic case of the special peak

The key features of each peak that needed to be determined were first to identify the dominant peak and then identify the upper and lower frequency range of the peak.

The first step in the processing was to curve fit the spectra with a second order polynomial. This was done for each of the synthetic spectra and then the curve fit was subtracted from the spectra. The results are shown in Figures 3.4-3.6.

In all cases there is a parabolic shape to the spectra. Note that a second order polynomial was used in the synthetic data and a second order polynomial was used to fit the complete synthetic data. The parabolic shape in Figures 3.4 to 3.6 shows that the fit is a poor representation of the polynomial in the synthetic data and this poor representation is caused by the peak.

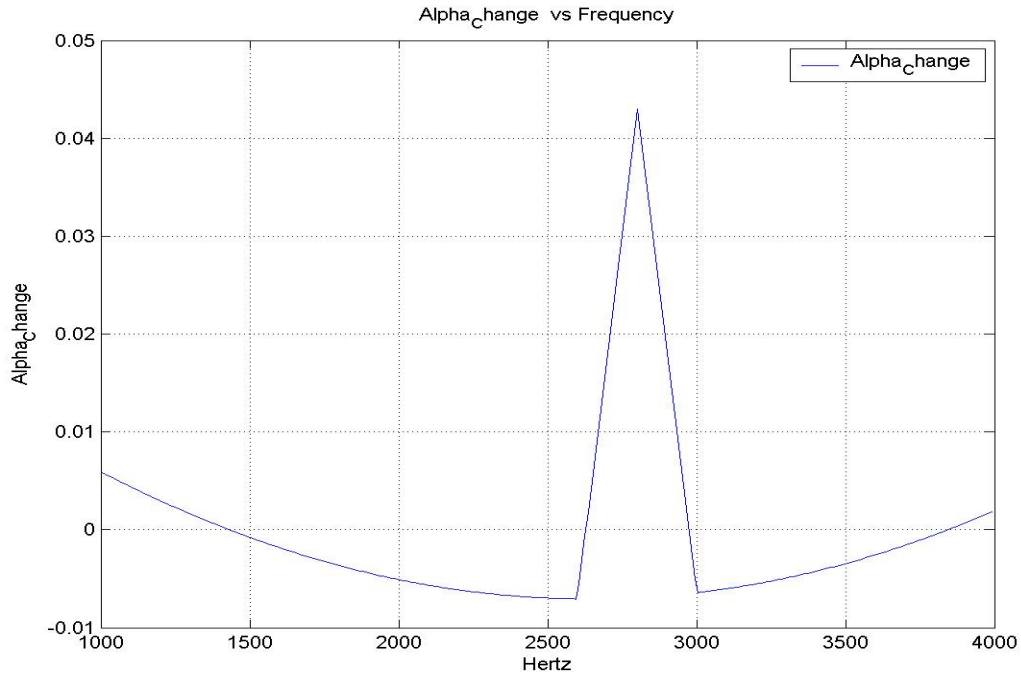

Figure 3.4: Difference between the simplified data with one peak from Figure 3.1 and the second order polynomial fit.

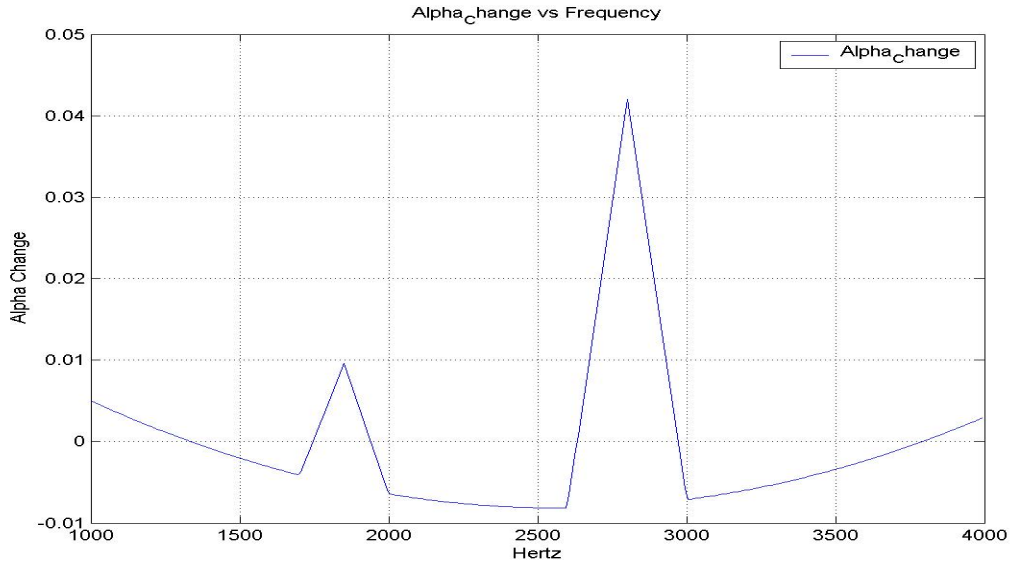

Figure 3.5: Difference between the simplified data with two peaks from Figure 3.2 and the second order polynomial fit.

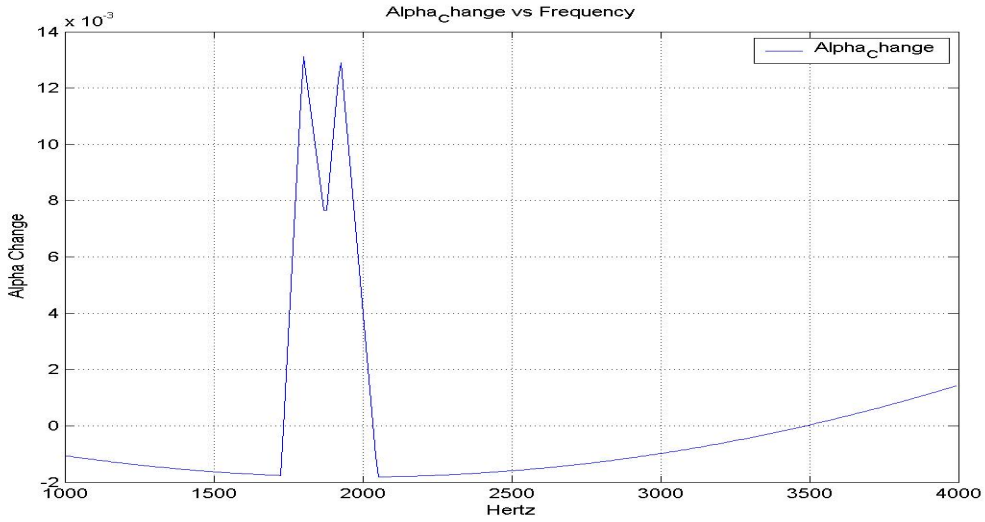

Figure 3.6: Difference between the simplified data with one peak from Figure 3.1 and the second order polynomial fit.

3.1.1 Identify Peaks

Each of the cases in Figures 3.4 to 3.6 represents different challenges. As a starting point consider the single peak case in Figure 3.4. While derivative calculations could be used to identify the peak, the real data would have many local minima and maxima that this was considered an inappropriate approach to identifying the peak.

The approach used to identify the peak was to identify the frequencies where the difference curve crosses zero. Figure 3.7 is a repeat of Figure 3.4 with the zero crossing, A, B, C, and D noted. Since with real data it was not expected that an exact zero would be

obtained, then a zero was defined as being between two consecutive points, one negative and the other positive.

The search for the zeros began by multiplying two consecutive data points. If the product of the two consecutive points was positive, then the two points were either both positive or both negative. And thus not considered a zero. However if the product of the two points was negative, then the first point was chosen to be the zero location if it is on the left side of the peak and the second point would be chosen if the zero on the right side of the peak that is being evaluated.

Note in Figure 3.7, that the peak is located between the zeroes labeled B and C. With four zeros marked A through D in Figure 3.7, the computer algorithm was to identify that zeros B and C has the peak in that range. In essence, a computer algorithm is needed to determine which zeros are paired, which represents a peak that will need to be removed.

Pairing the zeroes began with the two zeros with the lowest frequencies. If the value between them is below zero, then the pair does not contain a peak. If the value is positive then the peak value between the zeros are found. This process continues with each of the zero pair. For example in the case of Figure 3.7, zeros A and B are evaluated, B and C, and then C and D.

The algorithm scans through all the zeros starting from the lowest frequency. When a pair, such as B and C in Figure 3.7, has a peak identified then the amplitude, frequency of the peak, and the frequencies of the zeros are stored. Once all the peaks are identified, then the highest peak is identified for removal. Before removal, the true frequency range for the peak must be identified, because as seen in Figure 3.7, the zeros B and C do not represent the true range of the peak.

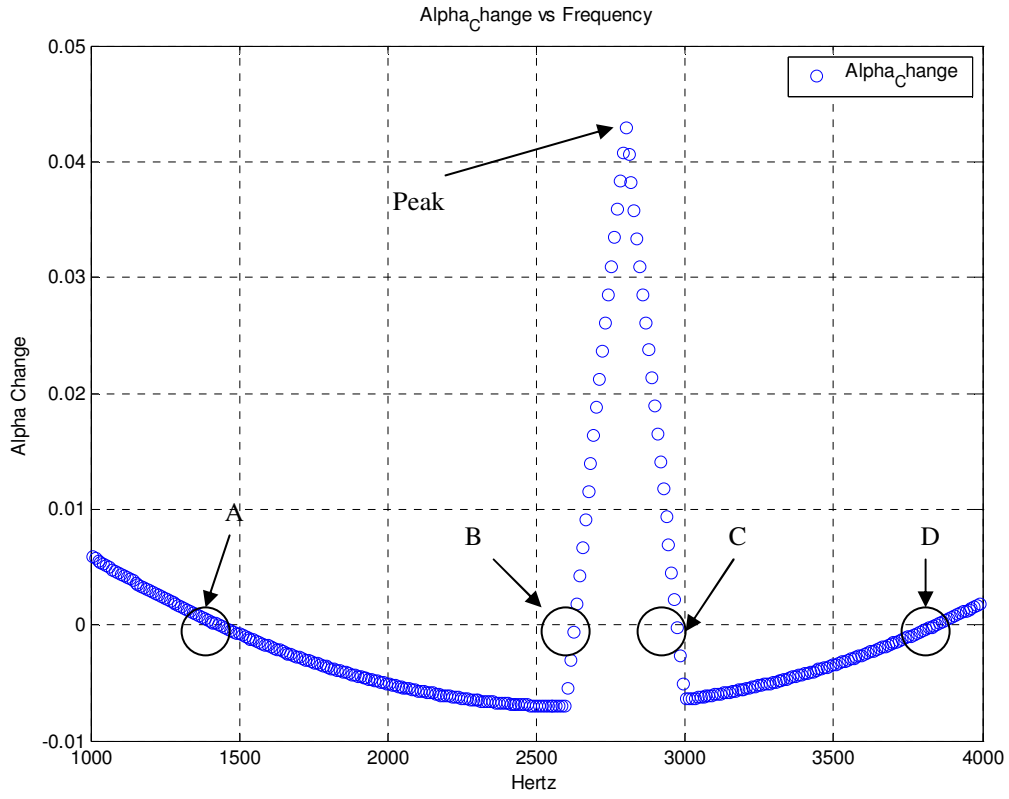

Figure 3.7: Difference between the synthetic data and the polynomial curve fit (Same as Figure 3.4). All the zeros are labeled.

3.1.2 Upper and Lower Limits

Once the peaks were found, the lower and upper limits needed to be identified as shown in Figure 3.8; these are always located to the left and to the right of the zeros used to identify a peak. Incorporating Rolle's Theorem the upper and lower limits will be where the slope is zero. Likewise the peak is located where the slope is zero. Therefore the zeroes of the slope are located at the lower limit, peak, and upper limit respectively. Figure 3.9, gives an example of the slope for the two peak synthetic data from Figure 3.5. The lower limit, peak, and upper limit frequencies for each peak are labeled.

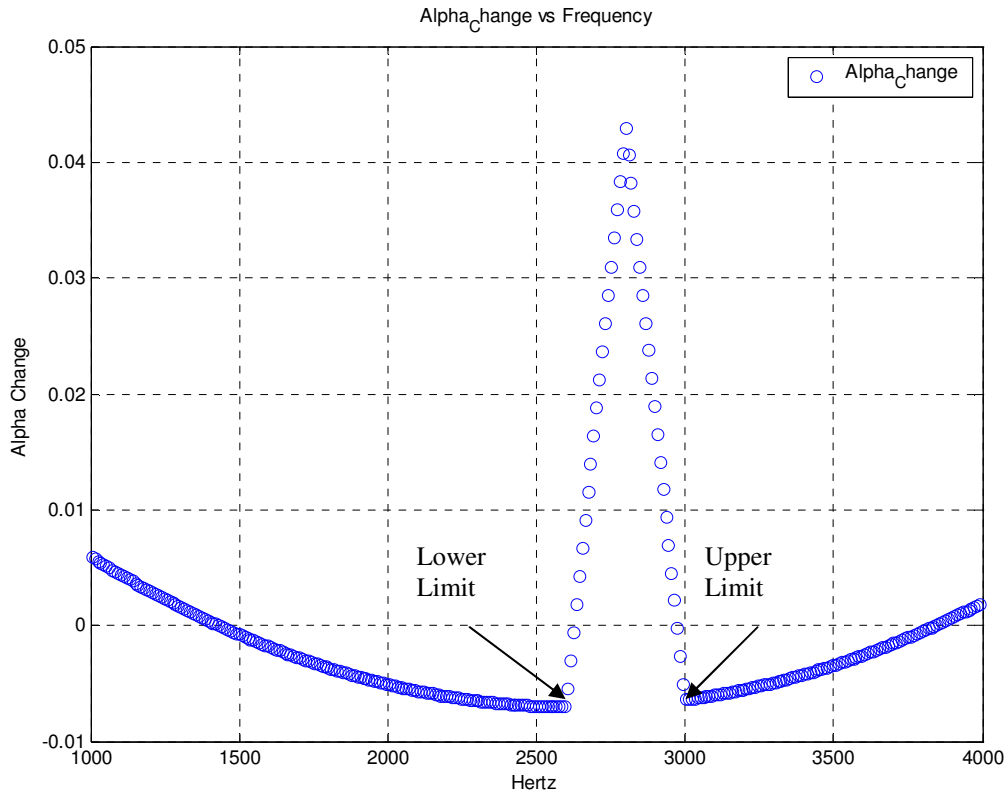

Figure 3.8: Synthetic data with the ideal lower and upper limits labeled.

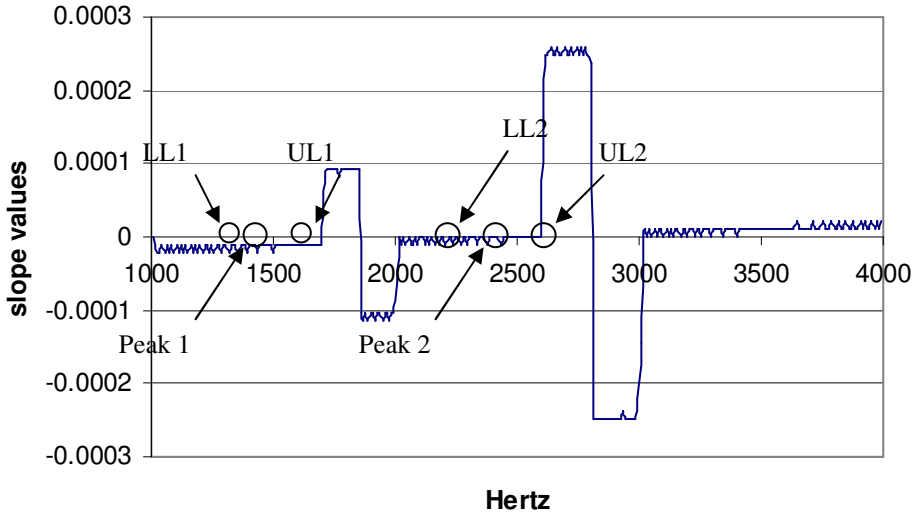

Figure 3.9: The slope of the double peak data from Figure 3.5. LL stands for lower limit and UL stands for upper limit

3.1.3 Removing Peaks

With the upper and lower frequencies of the peaks identified, the peaks can be removed. Removing the peak consists of replacing the values in the data with a linear line between the upper and lower frequencies. Without more information about the shape of the base curve and only given the two points, a higher order fit was not used. Further since the peaks do not cover large frequency ranges, the linear fit worked well.

Rather than removing all the peaks that were identified, one peak at a time was removed. This was done so that one could assess the presence of significant peaks in order to stop the peak removal process rather than remove very small peaks in the measured data.

As an example of the peak removal process, the simulated data for two peaks is shown in Figure 3.10. The goal was to remove the two peaks.

Figure 3.11 shows the simulated two peak data subtracted by a second order fit to the data. After the two peak frequencies were identified, a slope of the curve in Figure 3.11 was used to identify the upper and lower frequencies of each peak. Hence, the largest peak was then chosen for removal.

Figure 3.12 shows the simulated data with the largest peak removed. The second order curve fit is also shown. The process was repeated with the modified simulated data subtracted by the second order curve fit. The result in Figure 3.13 was then processed to identify the peaks. In this case only one peak was left. After removing this second peak, the remaining data and second order polynomial fit over lay each other, Figure 3.14, indicating successful removal of the peaks. Now the second order curve fit represents the background curve that needs to be subtracted from the original synthetic data to reveal the two peaks.

Figure 3.15 shows the synthetic data subtracted by the second order curve fit of the original data and then the fit to the data after removing both peaks. Figure 3.16 shows the second order polynomial obtained by removing the peaks and the polynomial before the peaks were removed. From the simulated data in Figure 3.10, the polynomial with the peaks removed better represents the baseline. These final results show that the two peaks are now accurately extracted from the synthetic data.

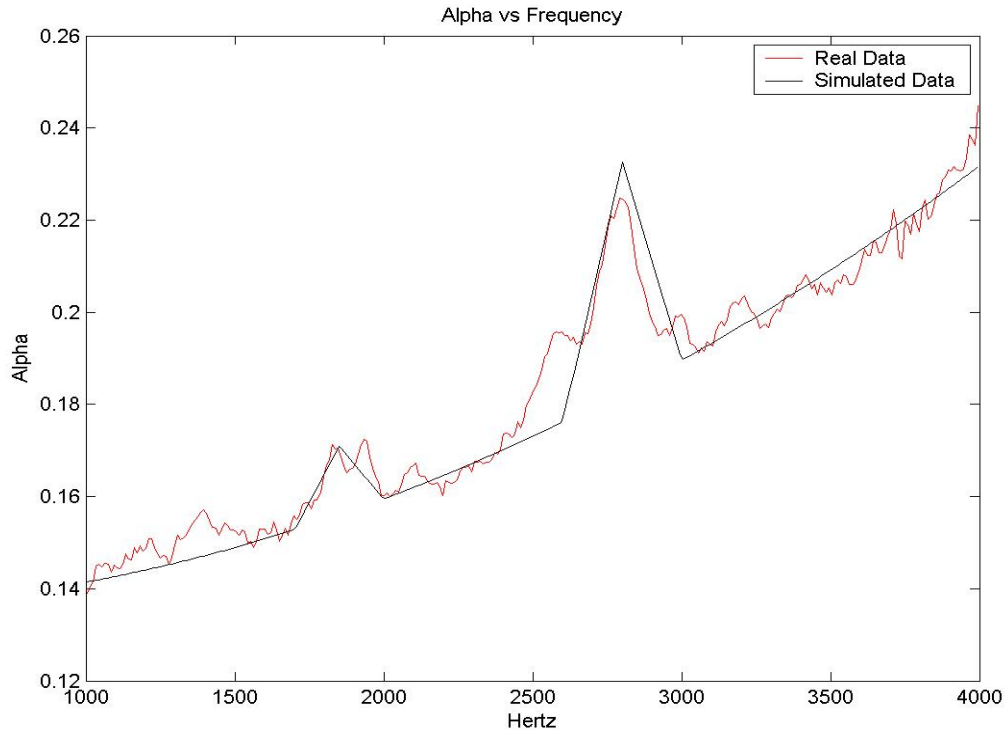

Figure 3.10: Initially the synthetic data has two peaks

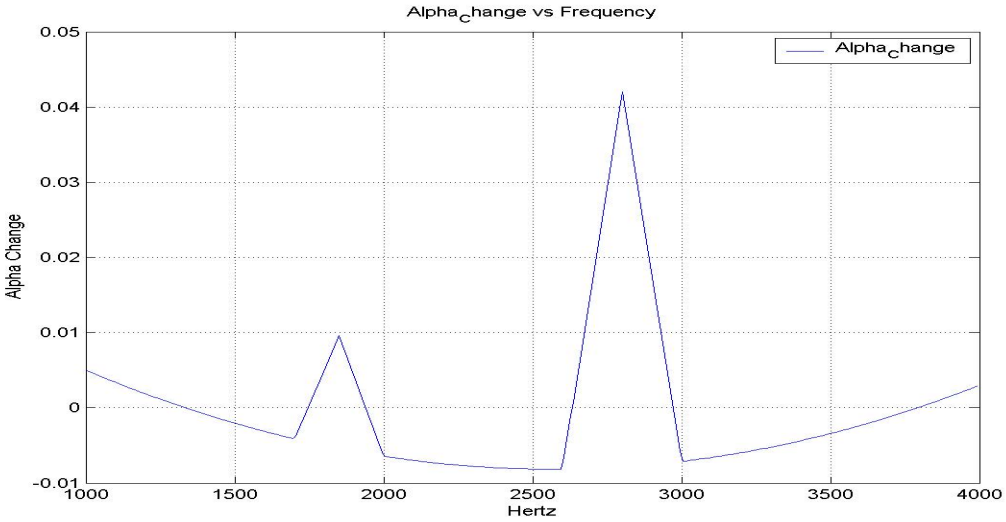

Figure 3.11: The data is then subtracted by the polynomial fit which results in the alpha change or deviation.

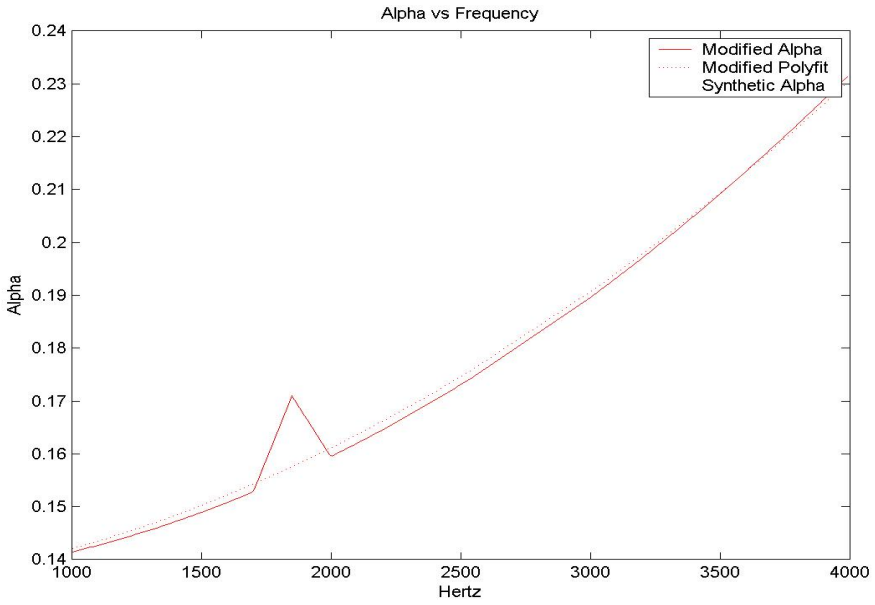

Figure 3.12: The peak of the most significance is removed and a new polynomial fit is applied.

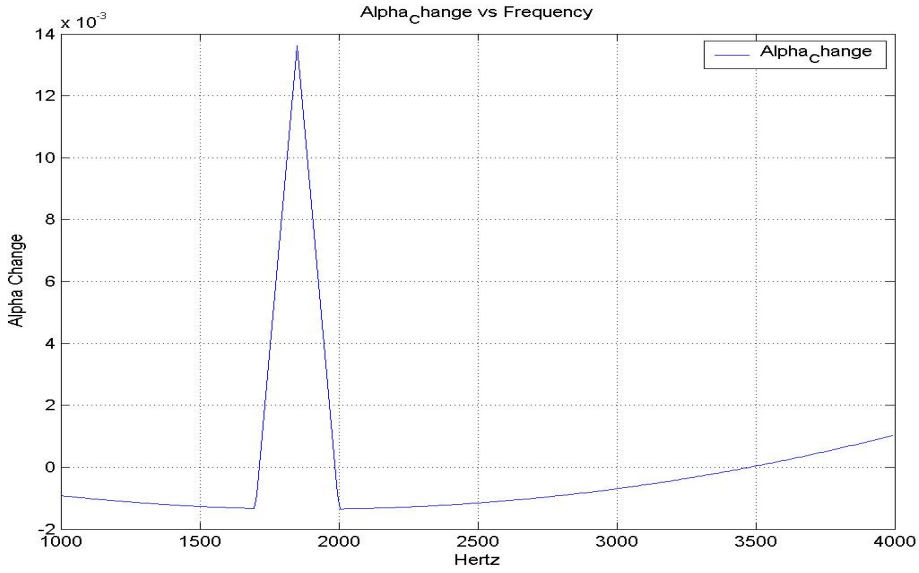

Figure 3.13: The synthetic data is subtracted by the new polynomial fit which gives another set of alpha changes.

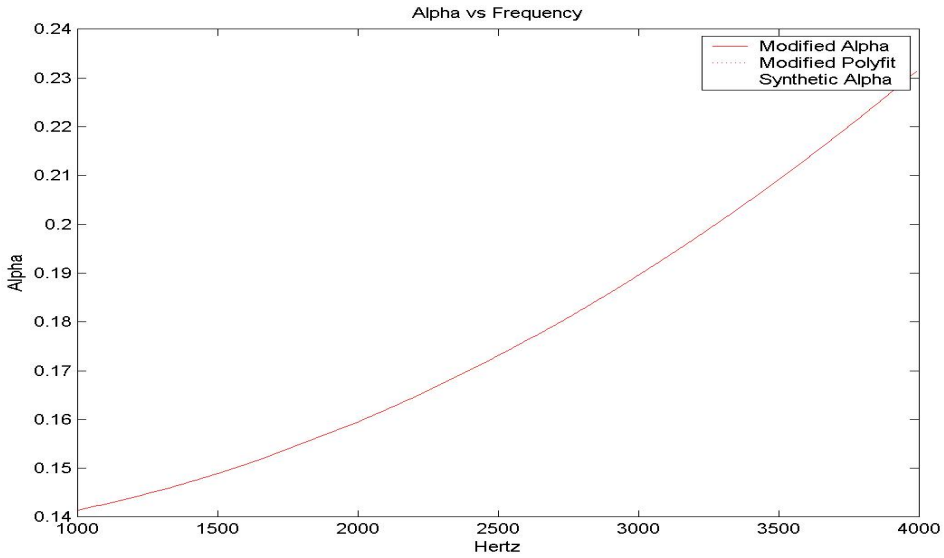

Figure 3.14: The final peak is removed and now the polynomial fit matches the base line curve.

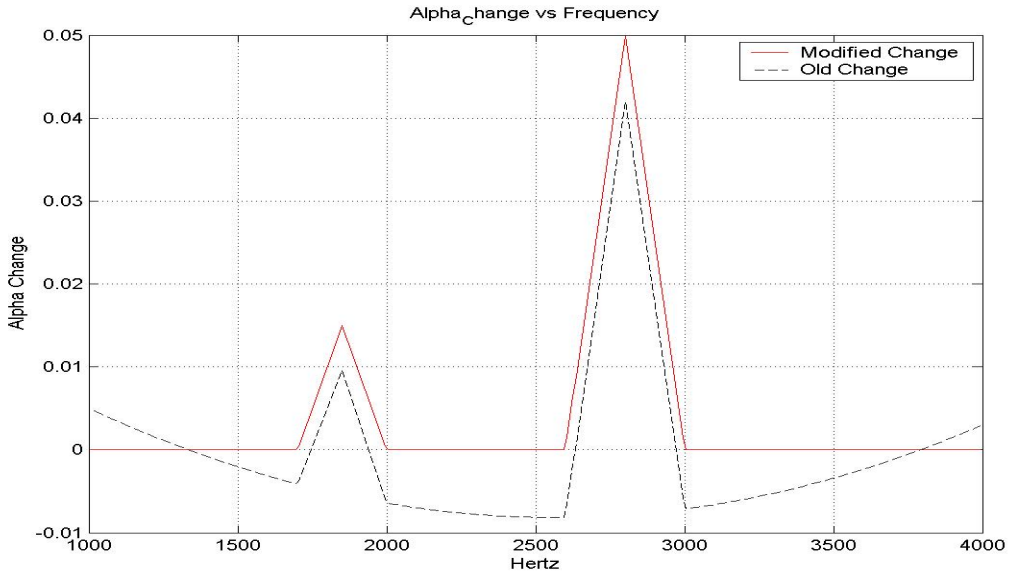

Figure 3.15: Comparison of the difference from the polynomial fit of the data with the peaks removed to Figure 3.12.

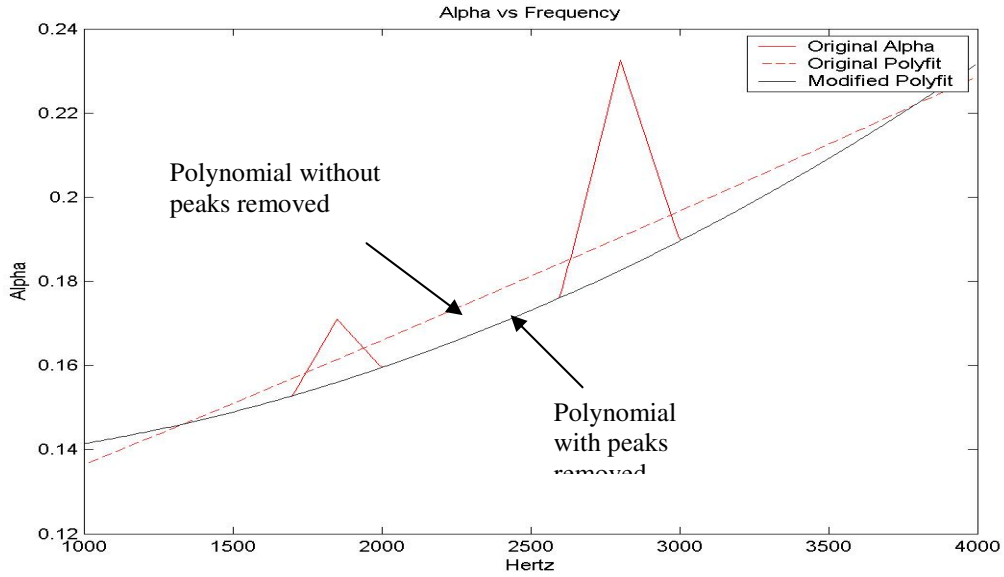

Figure 3.16: Comparison of the two polynomials with respect to simulated data in Figure 3.11.

In summary, the peak removal process devised from the synthetic data is:

1) Start with original absorption data
2) Second order curve fit
3) Subtract absorption data by curve fit
4) Identify all zeros
5) Identify zero pairs that bound a peak
6) Calculate the derivative of the curve from Step 3
7) Identify first zero slope from the left (lower limit) or from the right (upper limit) of the zero pairs that were identified as having the peak in the range.
8) Determine the highest peak

9) Replace the highest peak with a linear line between the upper and lower limits. Apply this to the absorption data
10) Repeat Steps 2 through 9 with the new absorption data until all peaks are removed.

The criteria for Step 10 will be discussed later with real data.

3.2 Real Data

After working with different cases of synthetic data, a proposed method was devised to be applied to real data. However because of the real data being less smooth than the simulated data, the process was modified to account for the behavior of the real data. This will bring the computer a step closer to automatically analyzing the data.

3.2.1 Transitional Problems

When using the method that was utilized in the synthetic data, there were difficulties caused by all the ridges and bumps in the real data. Figure 3.17, shows the peak removal process developed from the synthetic data applied to real data. The primary problem was that the upper and lower limits of each peak were not accurately identified because of the large number of local maxima and minima in the real data.

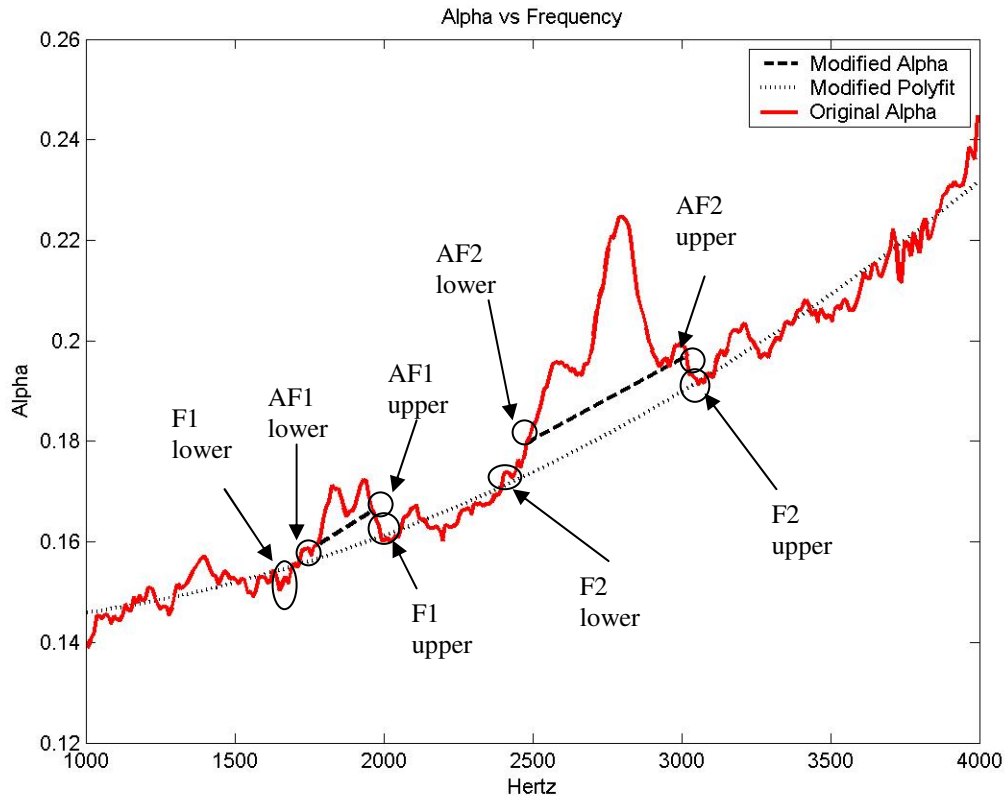

Figure 3.17: Real data with the peak removal method from the synthetic data being applied. The ideal upper and lower limits for each peak are labeled as F1 and F2; those automatically identified are labeled as AF1 and AF2.

In order to reduce the number of local maxima and minima, smoothing was used. The process of smoothing was a moving average where the number points in the average were examined. Smoothing over 3, 4, 5, 7, and 10 point was investigated. The smoothing was only applied to the data to identify the upper and lower frequencies, not to the data with peaks removed.

Figures 3.18 through 3.23 show results for an increasing number of points in the smoothing algorithm. In all these figures the curve labeled “Modified Polyfit” is the result after the peaks were removed carefully in a manual process, thus representing the ideal case. Comparing Figures 3.17 and 3.18, even 3 points of smoothing improves the identification of the upper and lower frequencies. Also note that three peaks are being removed. Finally in the case of 10 points for the smoothing, the upper and lower frequencies for each peak are identified as values near those from a manual process.

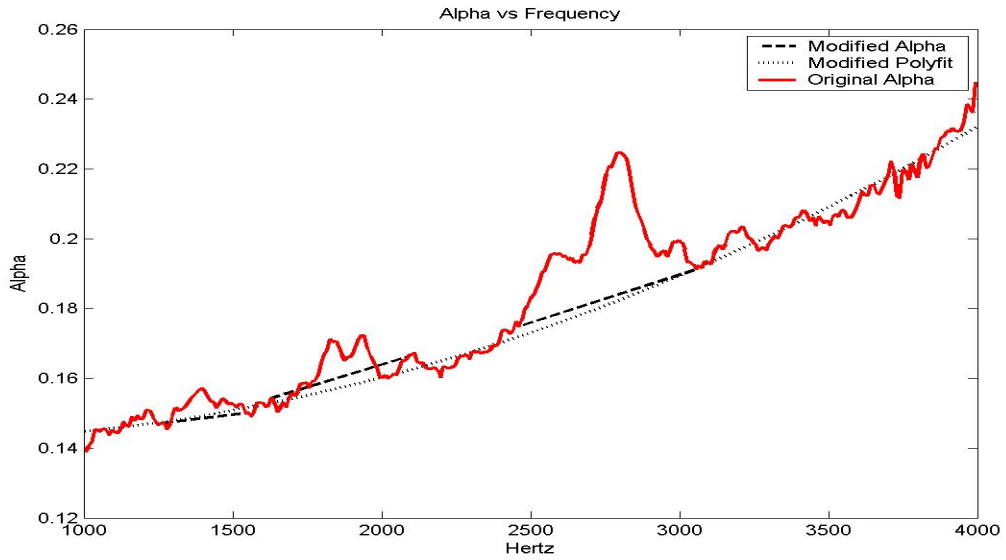

Figure 3.18: Peak removal with 3 point smoothing method

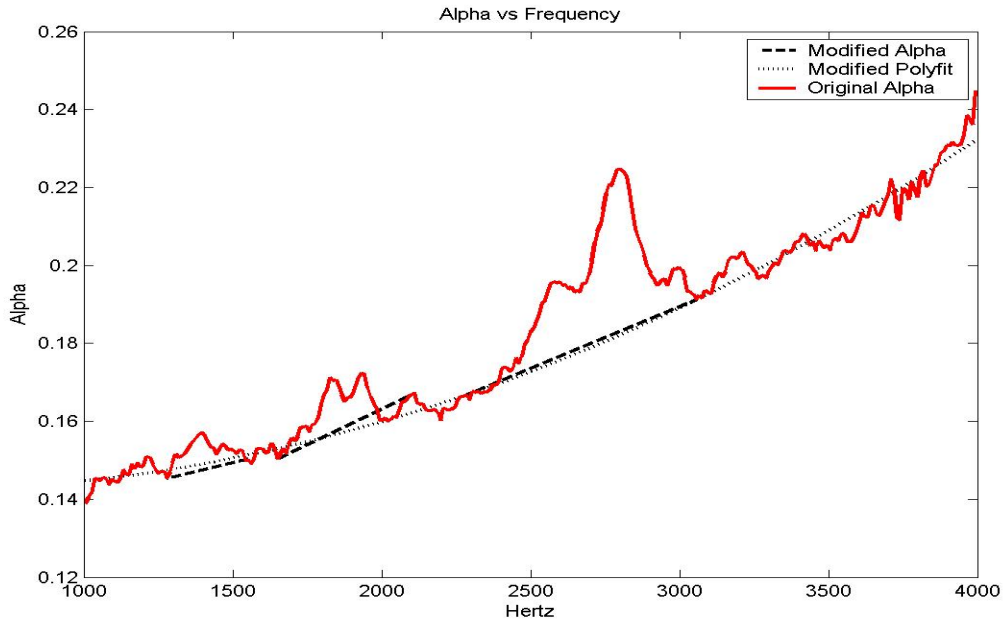

Figure 3.19: Peak removal with 4 point smoothing

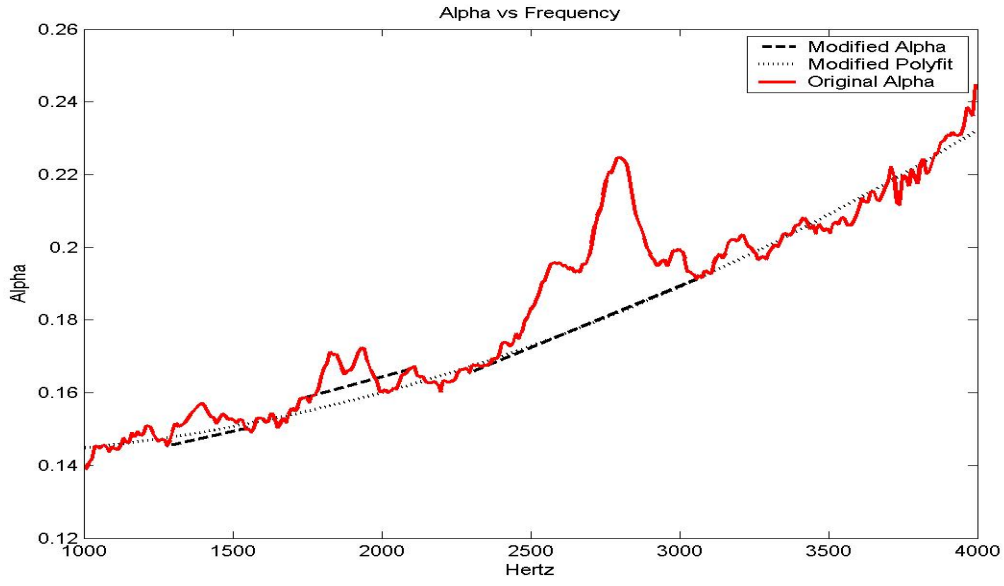

Figure 3.20: Peak removal with 5 point smoothing

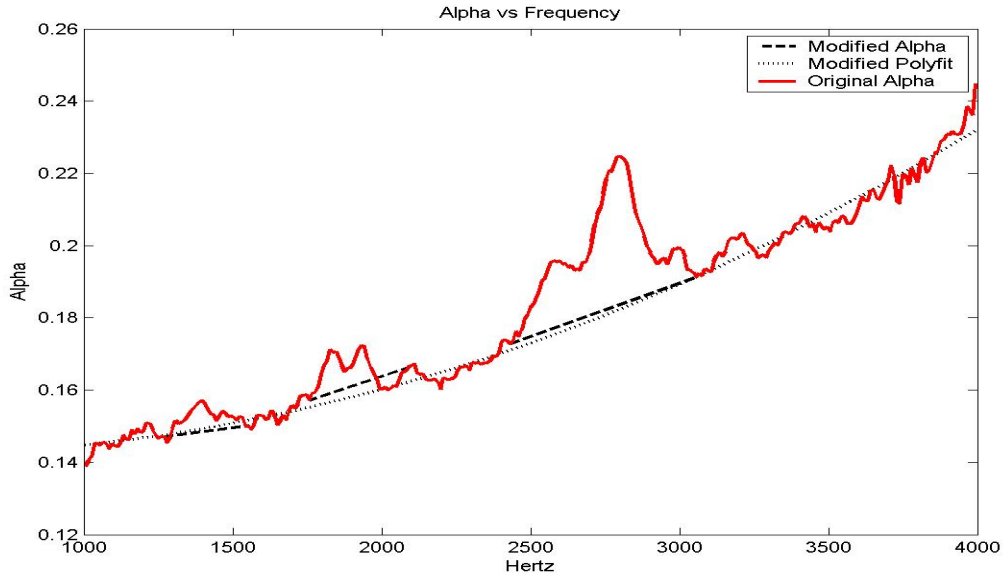

Figure 3.21: Peak removal with 7 point smoothing

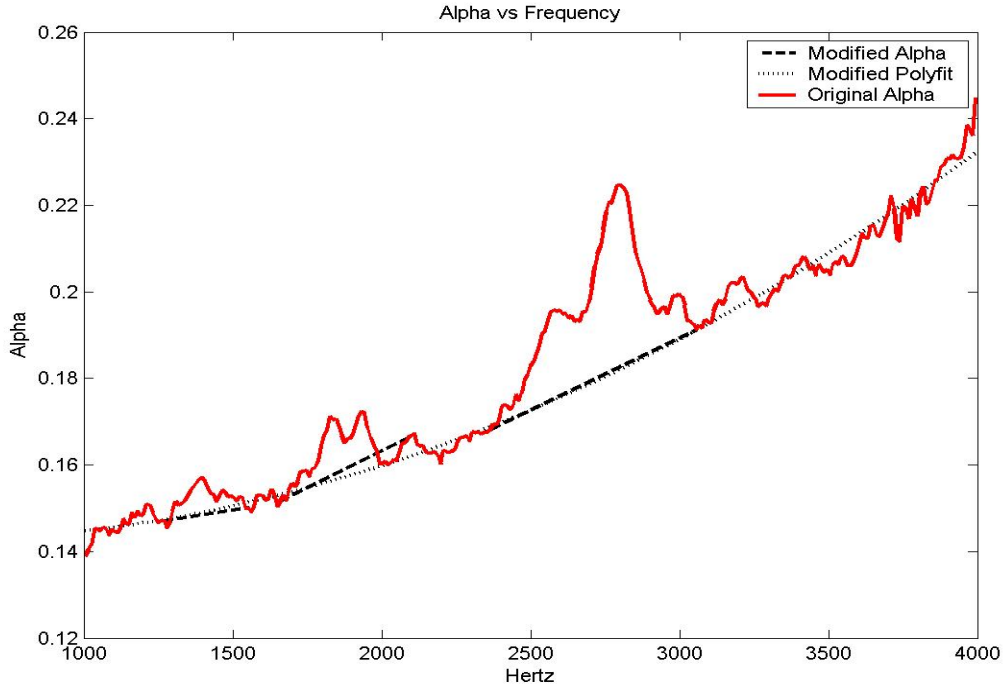

Figure 3.22: Peak removal with 9 point smoothing

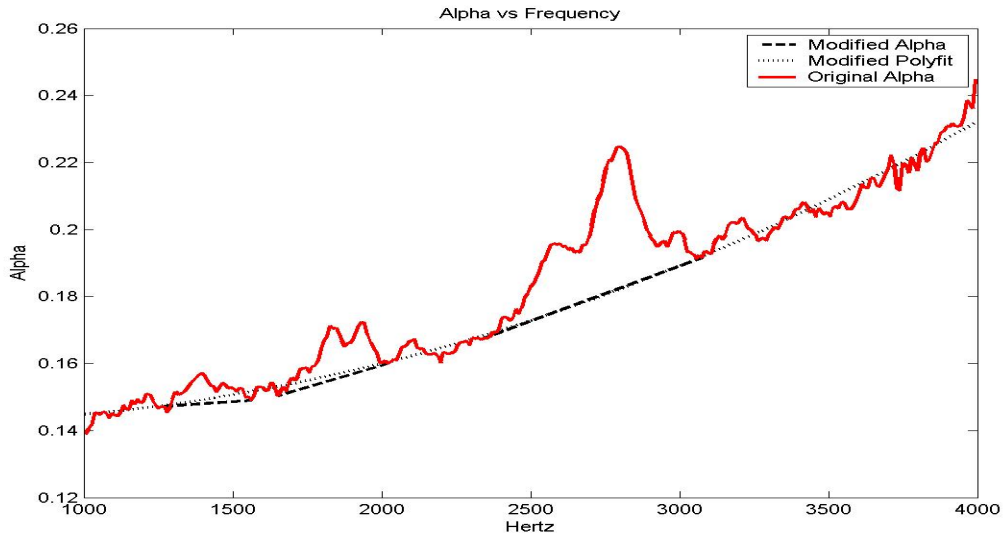

Figure 3.23: Peak removal with 10 point smoothing

3.2.2 Limiting Peaks Removed

When processing some of the defects there were still problems with getting the computer to identify which peaks were significant enough to remove. Without criteria, the computer could not distinguish a peak and random variation in data.

Initially, the criterion was the R-Squared value for the second order fit to the data. After a peak was removed, the resulting spectrum was fit with a second order polynomial and the R-squared value for the fit was examined. If it was greater than a set value, this indicated that any remaining deviation from a second order polynomial was random variation and not a clear peak. The R-Squared value that was used was 0.99 because that was the value of the correlation after the peaks were removed manually for several of the defects.

The R-squared method worked for most of the defect examples, but there were spectra for some defects that would not reach that value. It was also found that integration of the spectrum minus the polynomial over the range of the peak produced a negative number when an identified peak did not need to be removed.

After trial and error, set of three criteria were developed that successfully defined when the peak removal process had removed all significant peaks. Once any one of the following criteria was satisfied, the peak detection process stopped.

(1) a minimum peak value,

(2) the 2^{nd} order R-squared value after removing a peak

(3) and the value of integrating of the spectrum minus the polynomial curve fit over the frequency range of the peak.

To describe the minimum peak value, first the peak value is described. Figure 3.24 shows the different of the spectrum and the polynomial fit for synthetic data. The peak value is marked. The minimum peak value criteria is that if the peak value is below a set value, then the identified peak is not considered significant and the peak detection stops. To set the minimum peak value, the maximum peaks of all the defects were examined. Table 3.1 shows maximum peak value for each of the defects. In these cases, the peak for defect 1 had the minimum value and thus 0.0081 was assigned as the minimum peak value.

Finally after the peak is removed, the range was integrated. If the value was negative, then the peak removal process would stop. It should be noted that each criteria was looked at, and that any one of the criteria would be used to stop the peak removal process. Therefore, all three of the criteria were not checked in every case.

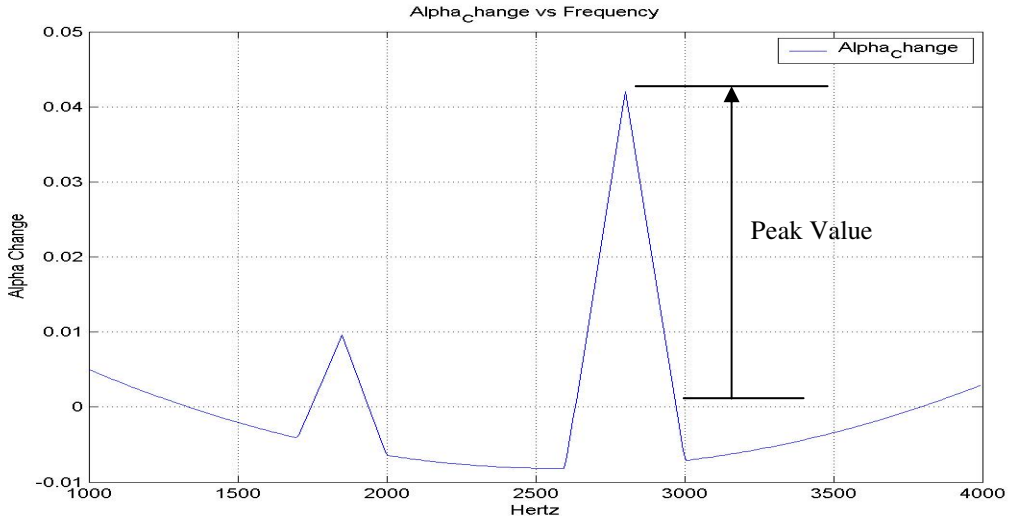

Figure 3.24: Figure 3.5 used as an example of how the maximum peak is calculated.

Using the three criteria, the automated process produced a polynomial curve fit as shown in Figures 3.25 and 3.26. Comparing the polynomial curve fit of the spectrum before and with peaks removed clearly shows in this case how the polynomial curve fit with peaks removed is an effective approximation to the baseline absorption spectrum. Figure 3.26 shows the curve that each peak was replaced with using the automated algorithm.

Table 3.1: The maximum value of the peaks in each defect, Defect 1 has the value of the least maximum peak, which is the value used as a criterion.

Defects	maximum peak
1	0.0081
2	0.0182
3	0.0182
4	0.0103
5	0.0156
6	0.0339
7	0.0096
8	0.0189
9	0.0334
10	0.0109
11	0.0208
12	0.0312
13	0.0174
14	0.0104
15	0.0099
16	0.0105

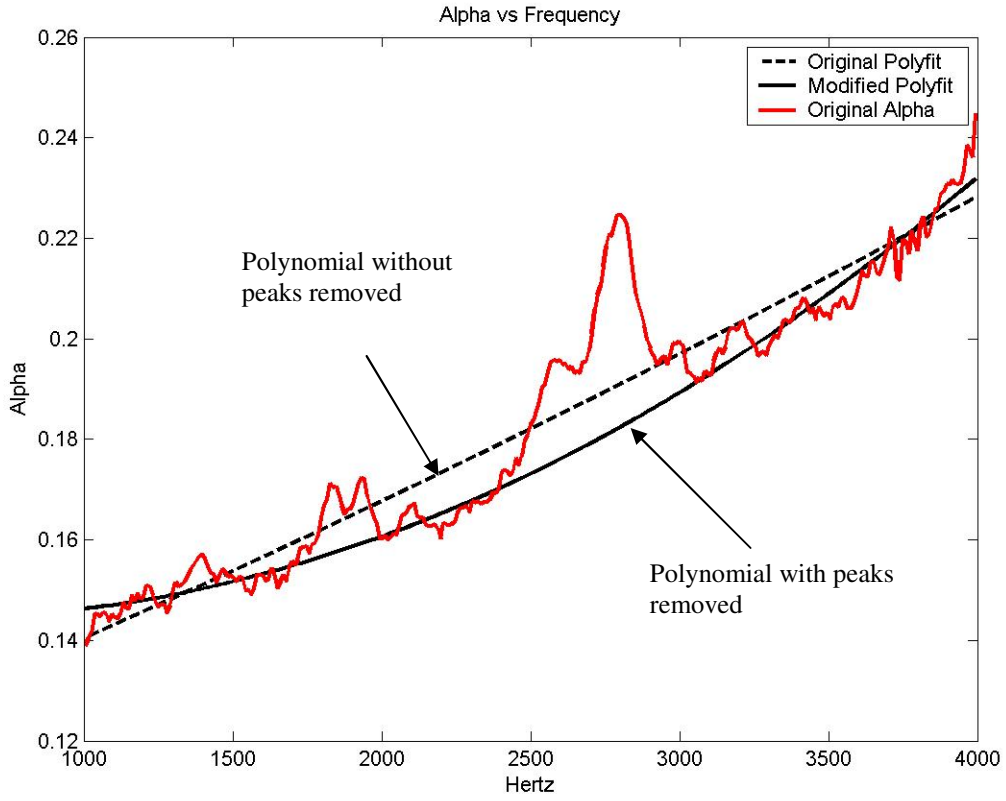

Figure 3.25: Final result of the peak removal of Defect 6 using a 10 point smooth with the criterions of R-Squared = 0.99 and peak size less than 0.0081.

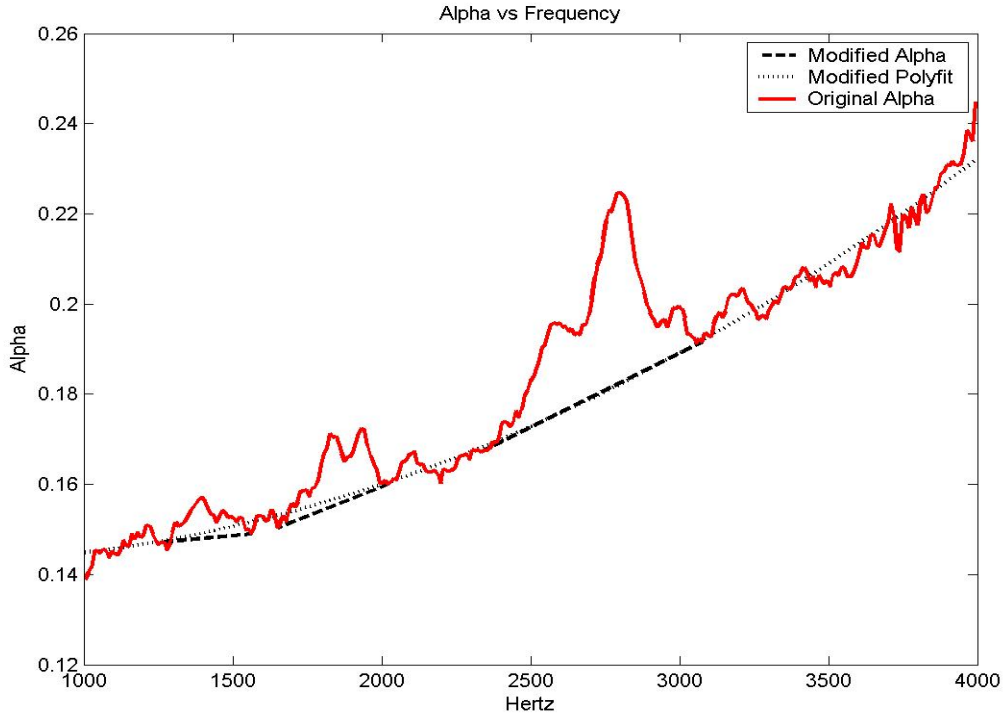

Figure 3.26: Final result of the peak removal of Defect 6 using a 10 point smooth with the criterions of R-Squared = 0.99 and peak size less than 0.0081. The same data as in Figure 3.26, but with the replacement for each peak shown

3.2.3 Final Results

Using the peak removal approach and the 10 point smoothing, Figure 3.25 shows the final result for the data over defect 6. The “Modified Polyfit” is now much better representation of the baseline curve and is significantly different than the second order polynomial fit to the original data (with peaks) which is labeled as “Original Polyfit”.

In addition to obtaining an improved representation of the baseline curve, the peak removal process has also defined the frequency ranges for all significant peaks in the data. Therefore the integration over a fixed frequency band in Thompson’s work can now be adjusted to the peaks that were identified for the removal. This choice of integration ranges was based on assuming that all peaks identified for removal were caused by the flaw, an assumption that has been supported by all the data obtained to date.

3.3 Summary

Figure 3.27 compares the method developed by Thompson (Previous Method) and the Proposed Method (Modified Method). The method to identify and then remove peaks from the measured sound absorption data was developed to handle typical variations from ideal data. Some of the processes are controlled by parameters that were set based on the available data. These may need to be changed to adapt these processes to other data range critical to the defect detection.

In the next chapter the peak removal tool is applied to additional flaws, and the results are compared to Thompson’s results.

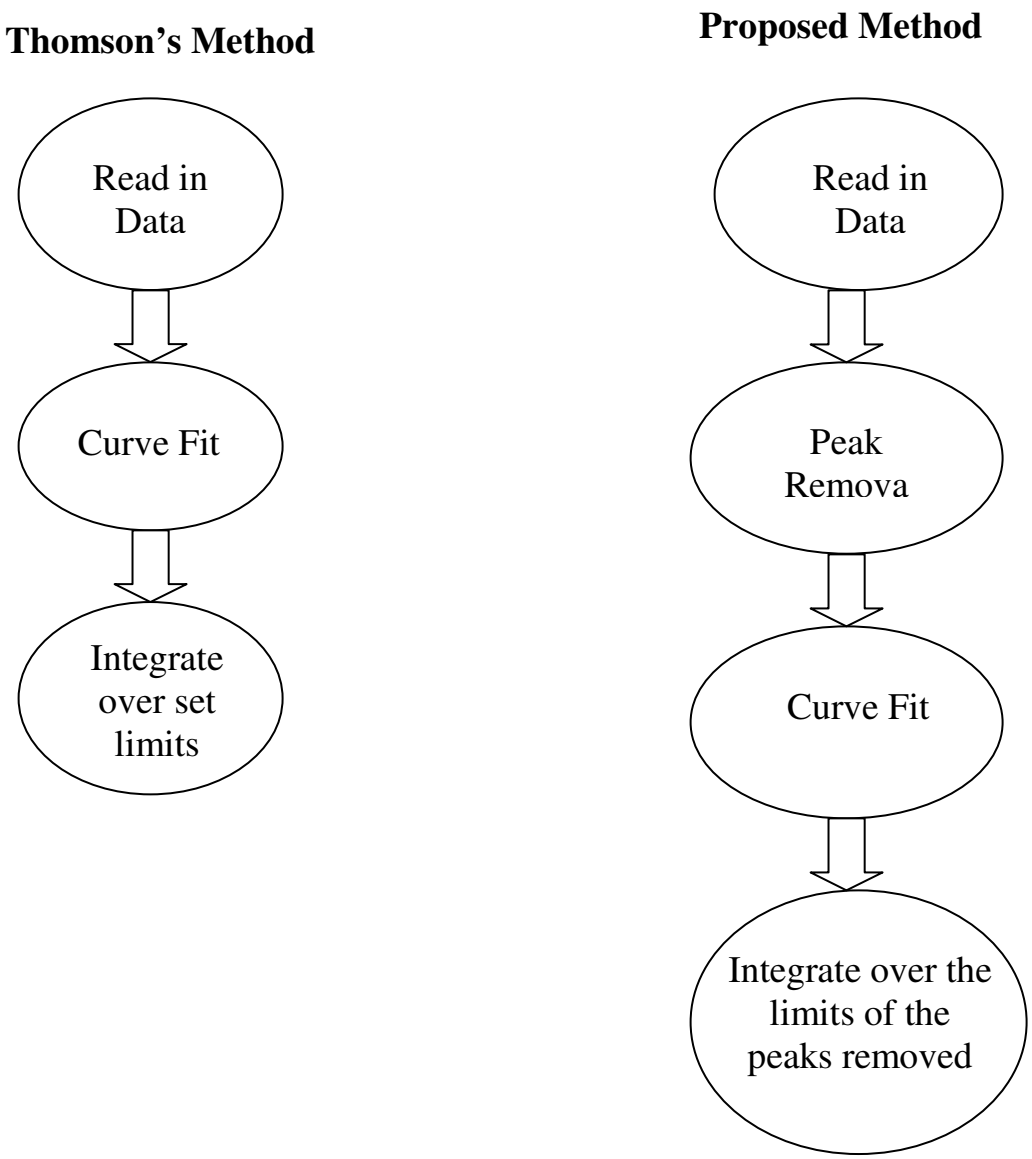

Figure 3.27: Block diagram of the flaw indicator methods. The left side is the approach that was taken by Thompson. The Right side is the Proposed Method approach.

Chapter 4: Results

The new automated peak removal method was applied to all the save data that Thompson used to develop his method. Therefore the results in this chapter only compare the data processing methods and not the difference in the data. The comparison will begin with the data from single point measurements and then the scans over an area. Each comparison was chosen to show the improvements caused by the peak removal and the integration frequency range. The results from each approach were labeled with the following names

Thompson: The method as developed by Thompson. Polynomial fit to the original spectrum (with peaks) and integration is over a fixed frequency range for all points.

No Peak: Thompson's method for polynomial curve fit to the original spectrum (with peaks) but with the integration over the frequency range of the peaks.

Hand: Peaks are removed by hand for the polynomial curve fit and integration is performed over the peaks.

Proposed: The full method developed in this thesis. Polynomial curve fit is applied to the spectrum with peaks removed, and integration is over the range of the peaks. The R-squared and integration criteria are applied to stopping the peak removal.

Table 4.1 summarizes the how different cases were chosen to show the influence of removing the peaks and the frequency range of integration.

Table 4.1 Naming convention for the methods compared in the result. Filled in cells indicated the cases run.

Name	Polynomial Fit Applied to Spectra			Integration for Indicator	
	With Peaks	With Peaks removed		Fixed Frequency band for all cases	Over frequency band of identified peaks
		Manual	Automated		
Thompson	■			■	
No Peak	■				■
Hand		■			■
Proposed			■		■

4.1 Single Point Comparisons

To begin the analysis of the various approaches, consider the comparison presented in Chapter 2: a comparison of Thompson's method (Thompson) and the manual method (Hand), Figures 4.1 and 4.2. Note that these are repeats of Figures 2.12 and 2.14. In these results, it was shown that removing the peaks made it possible to identify several of the flaws that were not identified with Thompson's method.

As shown in Figure 4.1, although the proposed method operated manually produced better results than Thompson's Method, the proposed method operated manually would still not detect all the defects. Therefore improvement still needed to be made.

Figures 4.3 and 4.4 show the results for Thompson's method with the integration over the peaks (No Peaks) compared to the results of the fully automated proposed method (Proposed). In all cases, the indicator value increases for the flaws compared to the hand method or Thompson's original method. However, the values over the bonded regions is sometimes lowered or raised. Therefore, integrating over the peak range is shown to be vital to improving the flaw indicator. The net results, is that with the proposed method, the flaw

indicator for each flaw is larger than any of the data over the bonded region. Thus, the proposed method is successful at identifying all of the defects. Further, this is clear evidence that removing the peaks before the polynomial fit is essential to produce a successful flaw indicator.

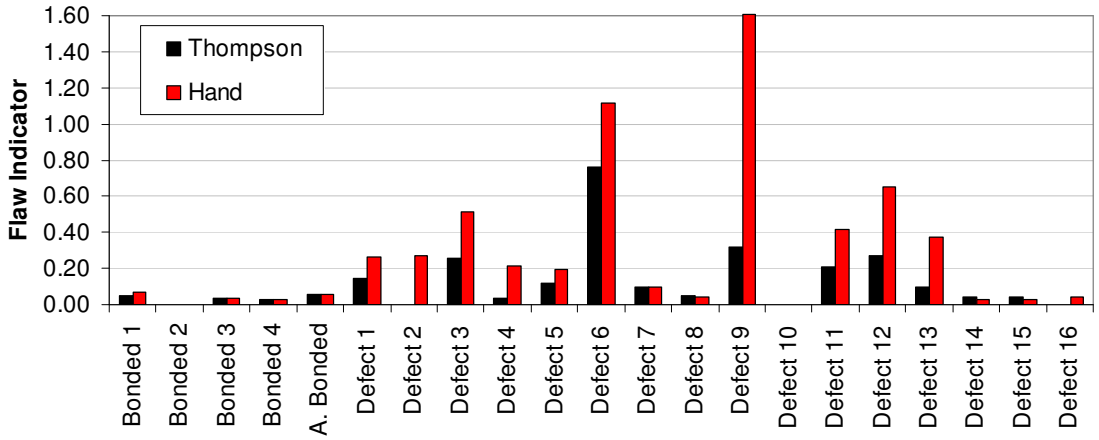

Figure 4.1: Comparison of the results from processing data over single flaws with Thompson's method and a manual process (Hand).

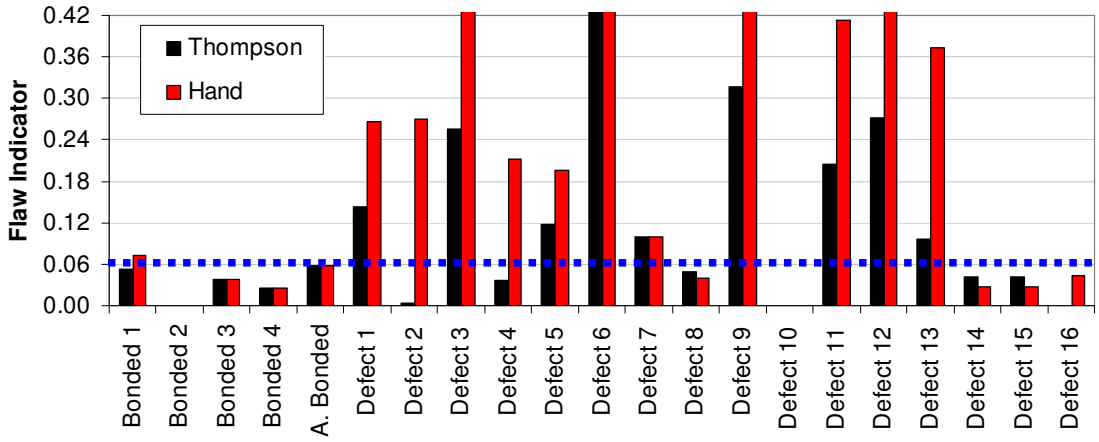

Figure 4.2: Same data in Figure 4.1 with a vertical axis chosen to zoom in on identifying the flaws.

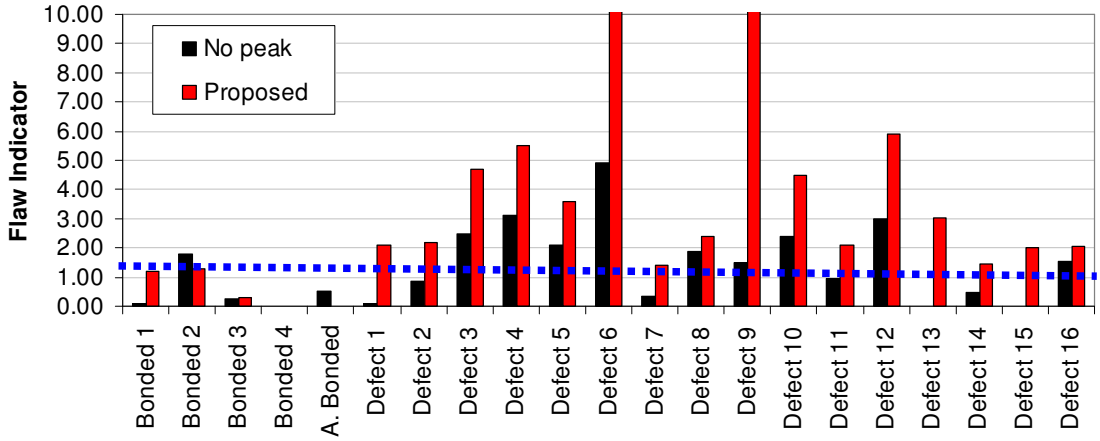

Figure 4.3: Comparison of the results from processing data over single flaws with Thompson's method and integration over the peaks (No Peak) and the proposed method (Proposed).

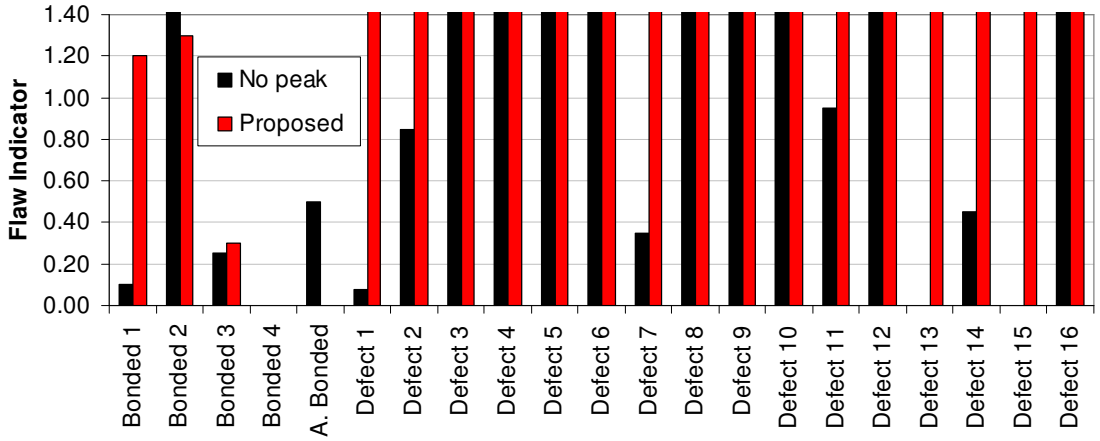

Figure 4.4: Same data in Figure 4.3 with a vertical axis chosen to zoom in on identifying the flaws.

Figures 4.5 and 4.6 compare the results for Thompson's original method to the proposed method. The proposed method does increase the flaw indicator value over the bonded regions. In two of the bonded cases, the value of the flaw indicator with the proposed method is larger than any of the values with Thompson's method. However, the values of

the flaw indicator increase much more dramatically over the regions with flaws. Thus, when comparing the flaw indicator value for the cases of the flaws to the values over the bonded region, all of the flaws are identified.

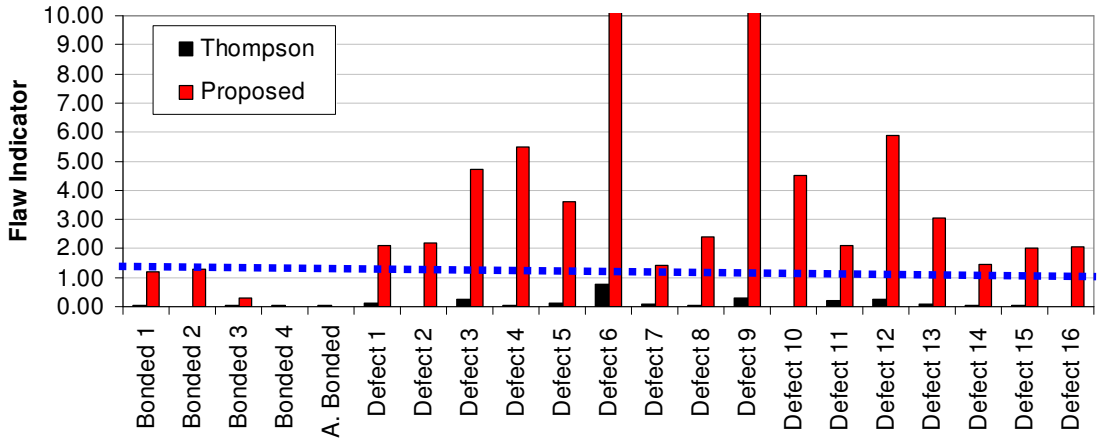

Figure 4.5: Comparison of the results from processing data over single flaws with Thompson's original method (Thompson) and the proposed method (Proposed).

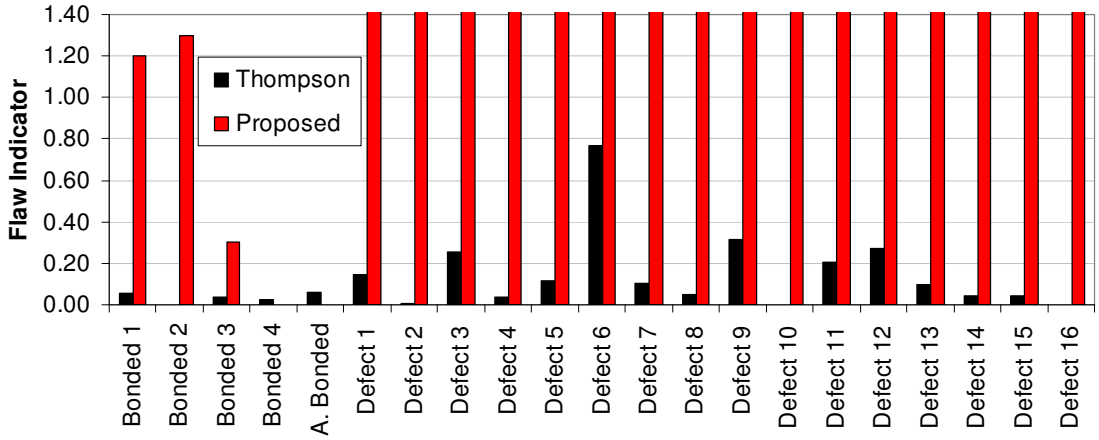

Figure 4.6: Same data in Figure 4.5 with a vertical axis chosen to zoom in on identifying the flaws.

Table 4.2 summarizes the success of each method to identify flaws. The proposed method was even better than the initial manual method and was capable of identifying all flaws. Further, by comparing the results from Figures 4.3 and 4.4 to the results in 4.5 and 4.6, it can be concluded that integrating over the range of the peaks was the most significant improvement, but not sufficient. Removing the peaks before the polynomial fit provided additional improvements to produce a method that identified all of the flaws.

Table 4.2: Summary of the flaws (defects) that were identified with each of the methods, a detected flaw is symbolized with an x.

Defects	Thompson	Hand	Proposed Method
1	X	X	X
2		X	X
3	X	X	X
4		X	X
5	X	X	X
6	X	X	X
7	X	X	X
8			X
9	X	X	X
10			X
11	X	X	X
12	X	X	X
13	X	X	X
14			X
15			X
16			X

4.2: Area Scans

The goal of a detection system would be to take data over an entire surface of a SOFI sample and then use the calculated flaw indicator to identify defects in the SOFI. This can be more challenging of a task than the single point measurements where it was known that the data was taken over a flaw.

Figure 4.8 shows an example of the flaw indicator on a scan of a seven by seven point grid over a flaw. The flaw indicator is represented with a false color plot. The plot shows the indications of a flaw on the right side of the area.

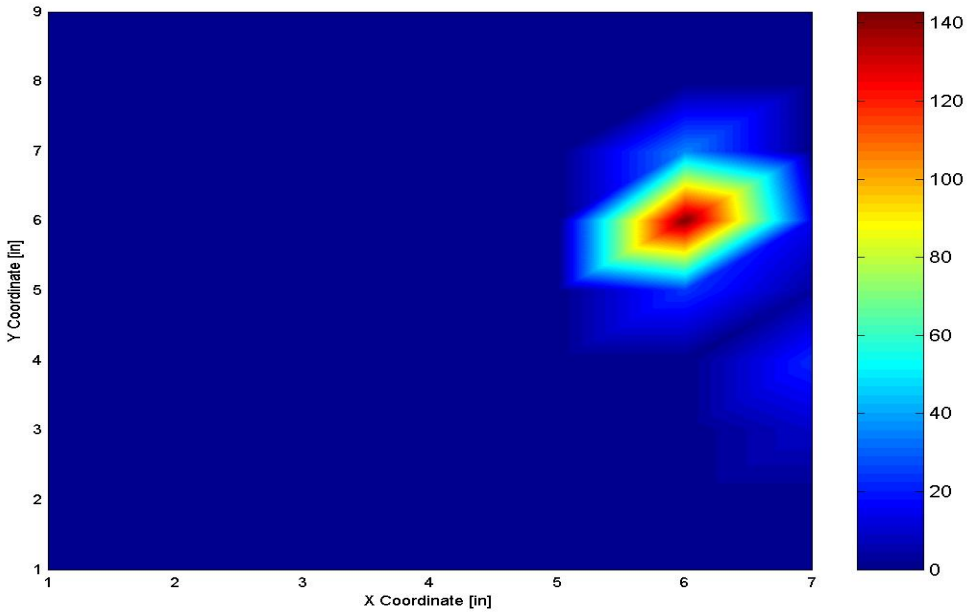

Figure 4.8: An example of a scan over a SOFI sample. The flaw indicator was calculated using the proposed method.

Figures 4.9 and 4.10 compare the results for scans processed with the proposed and Thompson's method respectively. While Thompson's method does identify defects 9 and 12, there is not the resolution to also identify defect 7. However, with the proposed method, defects 9 and 12 are identified along with defect 7. There is a third potential defect identified with the proposed method. It was indicated by the NASA persons that were involved with preparing the sample, that there could have been additional flaws in the sample. Further work would need to be done to determine if the large flaw indicator value to the right of defect 7 in Figure 4.9 is a true flaw or a false indication of flaw.

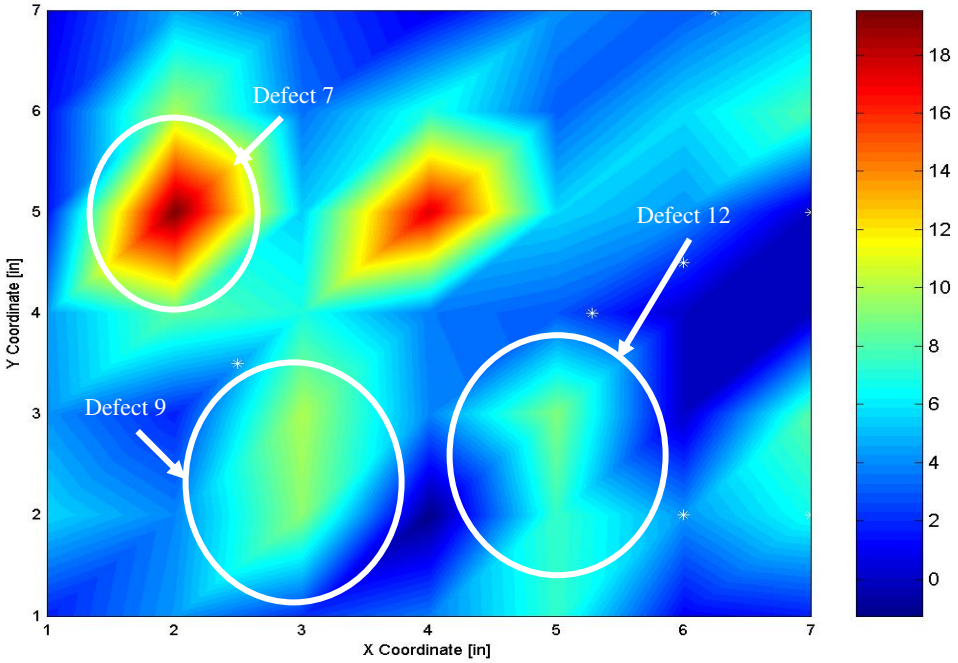

Figure 4.9: A scan that represents Defect 9 and 12 scan using the proposed method.

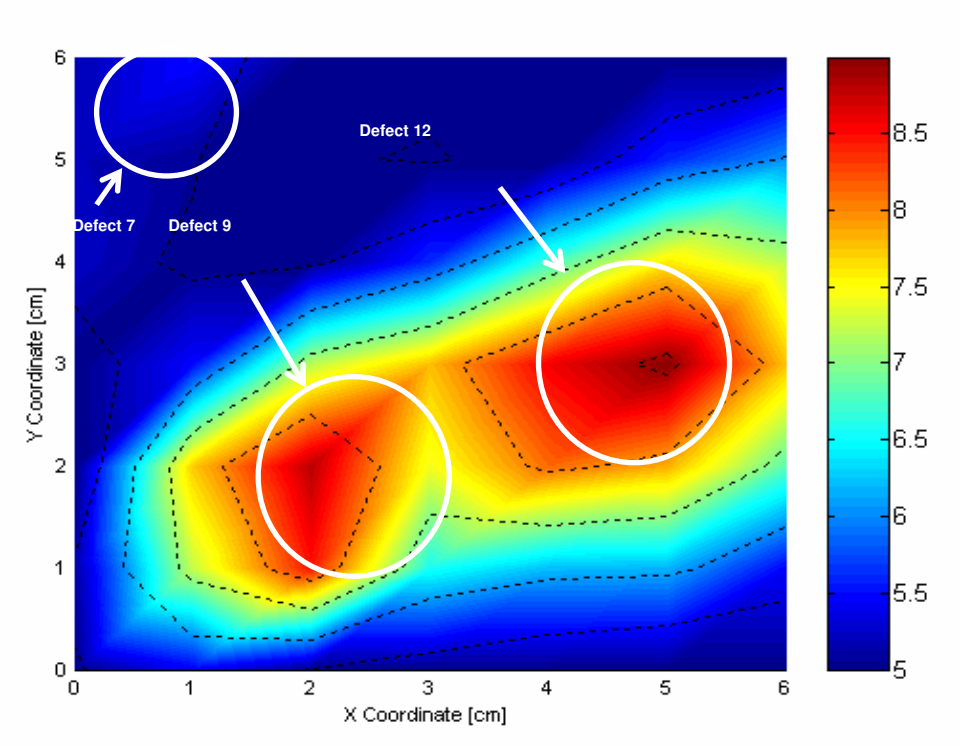

Figure 4.10: Scan of the area where Defect 9 and Defect 12 are located using Thompson's approach.

Figures 4.11 to 4.13 provide more comparison of Thompson's and the proposed methods applied to defect 1. In the case of Thompson's method, defect 1 could be identified, in Figure 4.11, but by scaling the plot , as in Figure 4.12, flow indicator values around defect 1 were highlighted. This was a concern at the time of developing Thompson's method. However for the new method,, Figure 4.13, the flaw indicator over defect 1 has a value that is significantly larger than the surrounding area and does not require a special plotting range for the defect to be visibly identified.

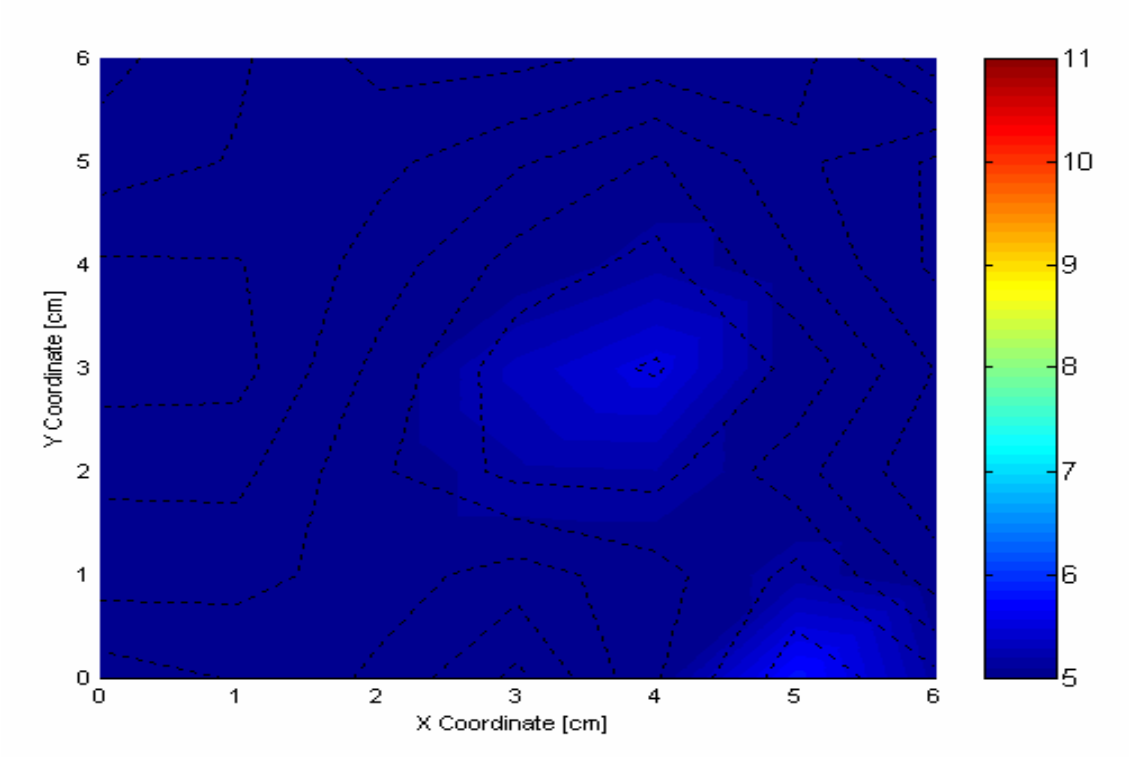

Figure 4.11: Defect 1 on a 6cm x 6cm scan using the previous method.

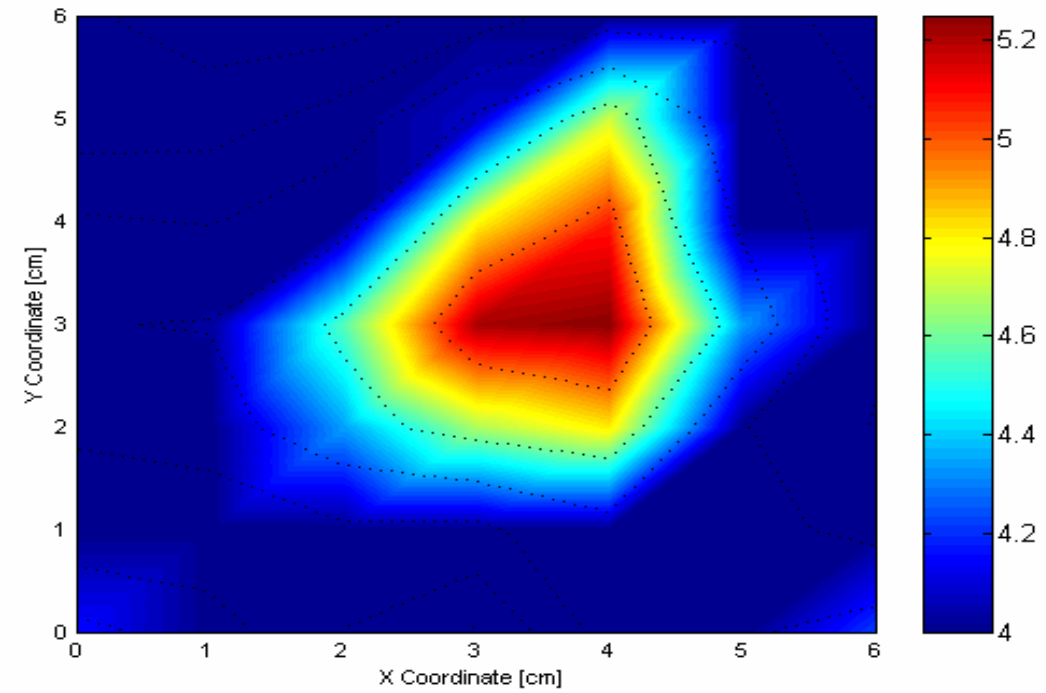

Figure 4.12: Defect 1 on a 6cm x 6cm scan using the previous method with a better resolution.

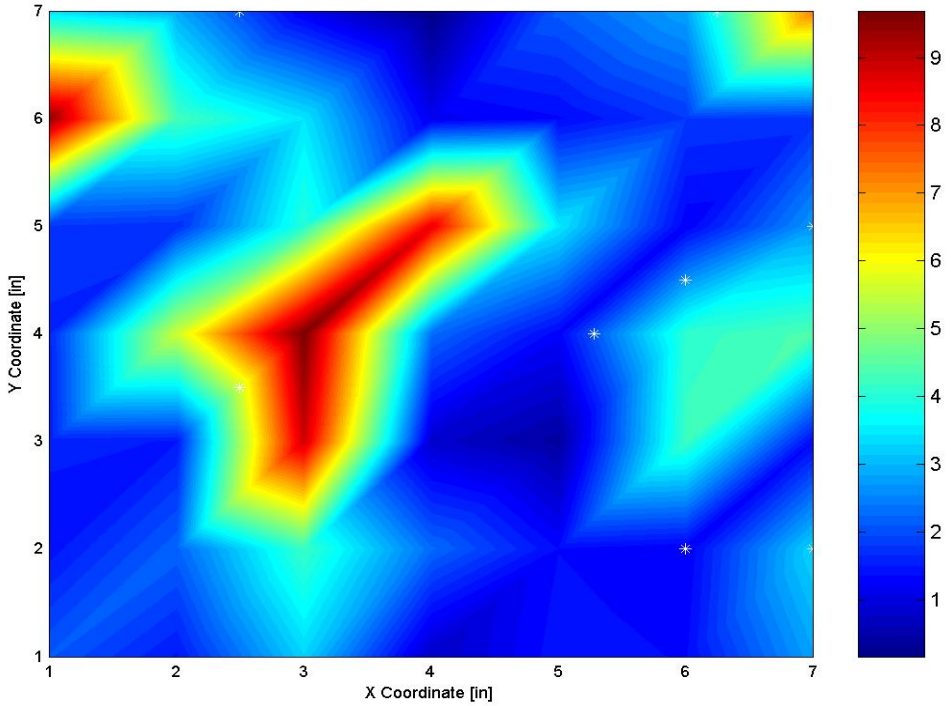

Figure 4.13: A scan that represents Defect 1 on a 6cm x 6cm scan using the proposed method.

4.3: Summary of the Results

Applying the proposed method to the single point methods showed that the proposed method produces a flaw indicator that is able to identify all defects when compared to SOFI regions where there are no known flaws. Further, when applied to data from several points over a SOFI surface, the proposed method produces results that do not need careful variations of the plotting range for the defects to be identified. However, the results do indicate that there is potential for false indications of defects or that there are more defects in the sample than were designed into the SOFI sample being tested.

Chapter 5: Summary and Conclusions

After the failure of the Columbia, NASA had investigated the reason why the space shuttle was destroyed and found that the dislodged pieces of SOFI were the cause. Therefore, efforts were increased to develop a method to determine whether the SOFI had bonded when sprayed on or a spot was missing. The technique explored in this thesis is an audio frequency absorption which could be a cost efficient and portable method. Previous work by Thompson (2005) developed the technique into one that was successful; however it did not work in all cases. Since some of the defects not detected were deemed significant, a more robust method of detecting defects was needed to be implemented. Therefore the goal of the work described in this thesis was to develop a new data processing method to improve upon the already existing method developed by Thompson.

Thompson's method focused on identifying deviations in the sound absorption spectrum measured over the SOFI sample. The deviation was in the form of peaks over limited frequency bands. The peaks could be identified as a deviation from a baseline spectrum that Thompson showed was fit well by a second order polynomial.

Initially, the measured sound absorption spectra were inspected manually to see if the method by Thompson could be improved. There was promise shown by removing the peaks. When the peaks were removed, the polynomial fit tended to better represent the baseline curve. The peaks would then standout as a larger deviation from the baseline curve, acting as a better way of detecting defects. However, it would be very tedious and time consuming for a person to remove the curves manually and examine each point of a surface scan. Therefore an automatic process needed to be developed.

The measured absorption spectra over 16 defects in a SOFI sample served at the test data to develop the new method. However, there was also random variation in the data that would complicate the development of the methods to remove the peaks. While it would be important to develop a method that could work with the random variations, an approach was devised to first use synthetic data that contained the key features of the real peaks in the measured data.

Modifications were made to the automated process in order to be utilized in real data. Even though the method worked well with the synthetic data, the random variations made the method not work properly. Therefore, many components were examined.

One of which was smoothing of the data was implemented. The smoothing of the data helped to get over the complications that the random variations would cause. This also enabled the lower and upper limits of each peak to be better identified. This approached was used with the other 15 defects and similar results occurred. Therefore smoothing was an excellent approach since it enables the identification of the desired upper and lower limits without having to deal with the complication that random variations would bring.

Each peak was integrated over its upper and lower limits, and the integrated values of each peak were summed. This was done for all the defects and the bonded regions for reasons of comparisons. However there was another issue which arose, that was getting the program to stop removing peaks once all evvective peaks were removed. This was a problem because the integrated values of some the peak that were removed were negative numbers, which made the flaw indicator in bonded regions larger than some defects. Therefore three criteria were established for the algorithm to stop removing peaks.

The criteria that were:

1) The R-squared value (correlation between the polynomial fit and the spectrum after the peak was removed) equals to 0.99.
2) The height of the peak that is being removed have to be greater than 0.0081.
3) The integral over the peak of the polynomial fit subtracted by the spectrum must be positive.

Using the set criteria for the automated process all defects were detectied. In Figure 5.1, one can see that each defect can be detected and that the new method is more sensitive than Thompson's Method..

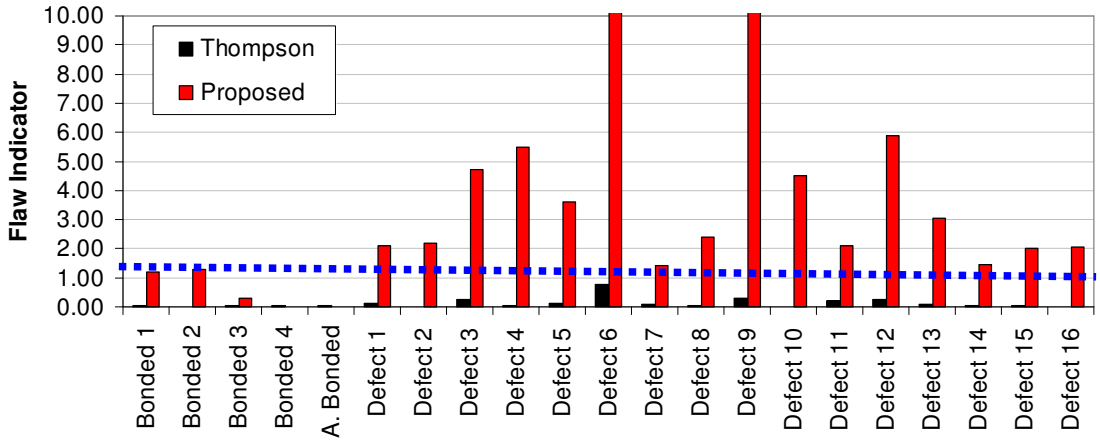

Figure 5.1: Comparison of the results from processing data over single flaws with Thompson's original method (Thompson) and the proposed method (Proposed).

When applied to data from several points over a SOFI surface, the proposed method produces results that do not need careful variations of the plotting range for the defects to be identified. However, the results do indicate that there is potential for false indications of defects or that there are more defects in the sample than were designed into the SOFI sample being tested.

5.1 Conclusion

In Conclusion, the Proposed Method is a more sensitive method for detecting defects. When the peaks are removed, the polynomial fit represents the baseline curve better therefore giving the user better resolution in detecting defects. In all the points, the Proposed Method detected each defect, Table 5.1. Looking at the mapping of the defects, Figure 5.2,, one would hope that large defects such as Defect 1, 2, 5, 6, 7 would be easiest to detect. Although Defect 5 and Defect 6 were detected using Thompson's Method, Defect 1, Defect 2, and Defect 7 were not detected. This also is more evidence that the Proposed Method is an improved method of detecting defects.

Table 5.1: A comparison of the defects that were detected using four different methods. X indicates detection

Defects	Thompson	Hand	Proposed Method
1	X	X	X
2		X	X
3	X	X	X
4		X	X
5	X	X	X
6	X	X	X
7	X	X	X
8			X
9	X	X	X
10			X
11	X	X	X
12	X	X	X
13	X	X	X
14			X
15			X
16			X

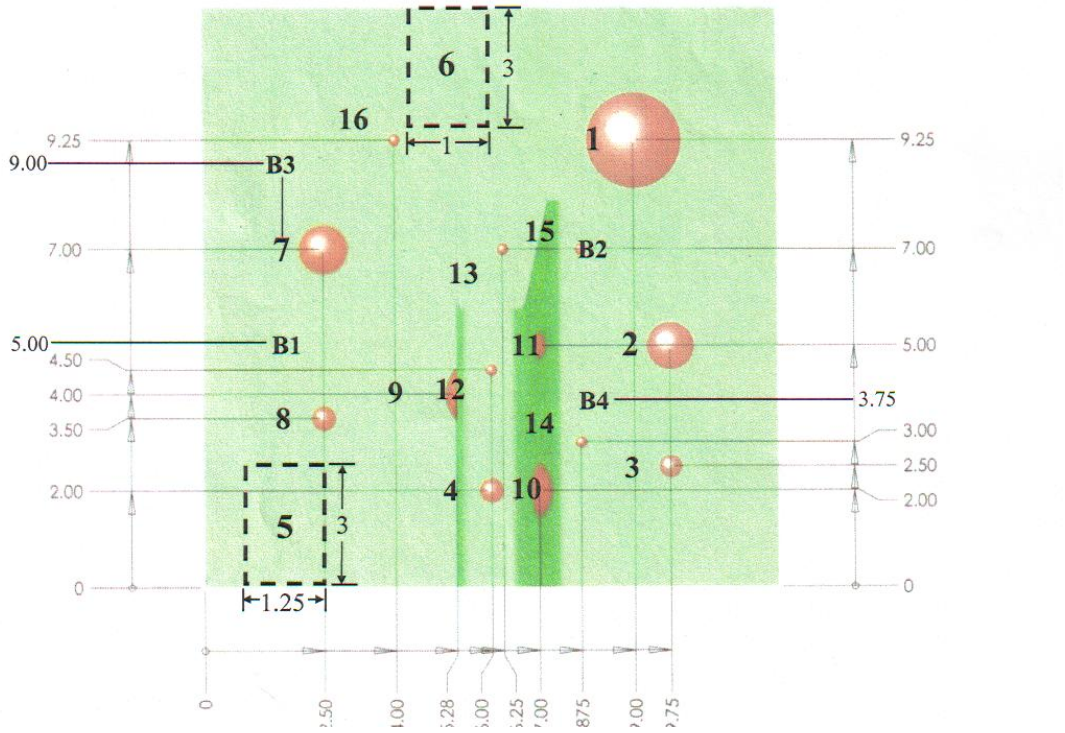

Figure 5.2: The map of all the defects and bonded regions in the foam.

5.2 Future Work

When incorporating the proposed method to the area scans, there was evidence that there were more defects than the 16 defects that were intentionally put in the sample during fabrication. Figure 5.3 is an example of a scan that contained Defects 1, 9 and 12. However there is another location (labeled "potential defect", where the flaw indicator suggest that there is a defect. Since this was not in the mapping of the embedded defects it must be determined if this is a false positive or indeed a defect that was not intended to be in the material. When asked about this, NASA engineers did not rule out the potential for such other defects.

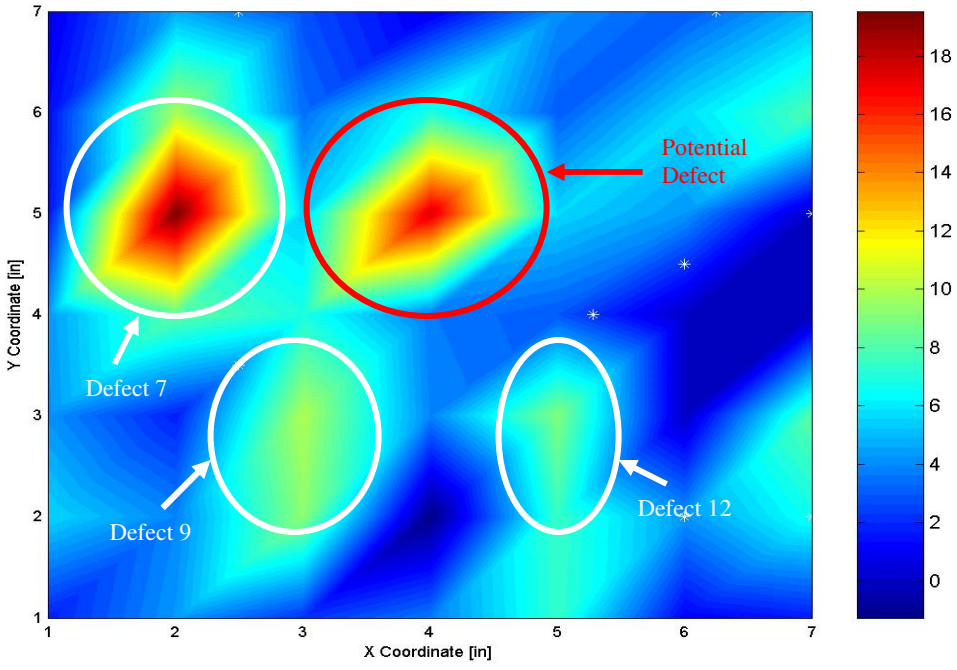

Figure 5.3: A scan that represents Defect 9 and 12 scan using the proposed method.

In addition to identifying defects, it would be important the further develop the method to classify the defect. Classification includes identifying the size, depth, and type of defect. Thompson did some limited work on this question, including the examination of the frequency of the peak as a means to classify the flaw depth. This initial work was not successful, but should be further pursued in the future.

Making samples were the defects are on top of each other would also be important to study in the future. An example of this would be to have Defect 5 and Defect 6 at the same position in the sample, but remain at their current depths: one in the middle of the sample thickness and one at the bottom of the sample. This will help to see if the Proposed Method would be able to detect the defects under those conditions.

Also other materials should be studied and see if the same method could be applied. The material will have to be one where sound waves can penetrate, which means the absorption coefficient of the material must below some limit. Further, the absorption coefficient should not be so low that changes cannot be detected. Studying different materials would help establish these limits in the absorption coefficient for the method to be usable. Also the material should not be hollow, but be a solid structure. Understanding all these limits could show the application of the flaw detection method to other applications.

References

1. Columbia Accident Investigation Board (2003). CAIB Recommendation R6.3-2. Retrieved on January 30, 2006.
2. Columbia Accident Investigation Board, (2003) Volume 1, Chapter 6, p. 138.Chapter 6; retrieved June 8, 2006
3. Columbia Accident Investigation Board (2003). Report of Columbia Accident Investigation Board, Volume I, chapter 6, page 173. Retrieved on January 4, 2006.
4. Columbia Accident Investigation Board (2003). In-Flight Options Assessment, Volume II, appendix D.12. Retrieved on January 30, 2006.
5. Columbia Accident Investigation Board (2003). Report of Columbia Accident Investigation Board, Volume I. Retrieved on January 4, 2006.
6. Columbia Accident Investigation Board (2003). Report of Columbia Accident Investigation Board, Volume I, chapter 3, page 78. Retrieved on January 4, 2006.
7. Columbia Accident Investigation Board (2003). Report of Columbia Accident Investigation Board, Volume III, Part 2, page 88. Retrieved on August 18, 2006.
8. ^ Chien, Philip (June 27, 2006) "NASA wants shuttle to fly despite safety misgivings." *The Washington Times*
9. ^ Foam still a key concern for shuttle launch. New Scientist SPACE. Retrieved on August 13, 2006.
10. McKee, Matt. "An acoustic impedance investigation of spray-on foam insulation to detect bonding condition", MS Thesis, Iowa State University, May 2004
11. Thompson, Todd A. "Evaluating the bonding condition of NASA spray on foam insulation using audio frequency sound absorption measurements", MS Thesis, Iowa State University, May 2005

Biographical Sketch

Gregory Stargell was born December 1, 1982 in Atlanta, GA. He received his Bachelor of Science Degree in Physics with a concentration in Computer Science from Alabama A&M University and Master of Science in Mechanical Engineering from Iowa State University. He served as a Research Assistant for The Mechanical Engineering Department in the Acoustics Lab.